

## Tropical Pangaeon Precipitation

N. G. Heavens et al.

# Glacial-interglacial variability in Tropical Pangaeon Precipitation during the Late Paleozoic Ice Age: simulations with the Community Climate System Model

N. G. Heavens<sup>1</sup>, N. M. Mahowald<sup>1</sup>, G. S. Soreghan<sup>2</sup>, M. J. Soreghan<sup>2</sup>, and C. A. Shields<sup>3</sup>

<sup>1</sup>Department of Earth and Atmospheric Sciences, Cornell University, Ithaca, New York, USA

<sup>2</sup>ConocoPhillips School of Geology and Geophysics, University of Oklahoma, Norman, Oklahoma, USA

<sup>3</sup>Climate Change Research Section, Climate and Global Dynamics Division, National Center for Atmospheric Research, Boulder, Colorado, USA

Received: 18 April 2012 – Accepted: 14 May 2012 – Published: 25 May 2012

Correspondence to: N. G. Heavens (heavens@cornell.edu)

Published by Copernicus Publications on behalf of the European Geosciences Union.

Title Page

Abstract

Introduction

Conclusions

References

Tables

Figures

◀

▶

◀

▶

Back

Close

Full Screen / Esc

Printer-friendly Version

Interactive Discussion



## Abstract

The Late Paleozoic Ice Age (LPIA), the Earth's penultimate "icehouse climate", was a critical time in the history of biological and ecological evolution. Many questions remain about the connections between high-latitude glaciation in Gondwanaland and low-latitude precipitation variability in Pangaea. We have simulated the Earth's climate during Asselian-Sakmarian time (299–284 Ma) with the Community Climate System Model version 3 (CCSM3), a coupled dynamic atmosphere-ocean-land-sea-ice model. Our simulations test the sensitivity of the model climate to direct and indirect effects of glaciation as well as variability in the Earth's orbit. Our focus is on precipitation variability in tropical (30° S–30° N) Pangaea, where there has been the most interpretation of glacial-interglacial climate change during the LPIA. The results of these simulations suggest that glacials generally were drier than interglacials in tropical Pangaea, though exceptional areas may have been wetter, depending on location and the mode of glaciation. Lower sea level, an indirect effect of changes in glacial extent, appears to reduce tropical Pangaeian precipitation more than the direct radiative/topographic effects of high-latitude glaciation. Glaciation of the Central Pangaeian Mountains would have greatly reduced equatorial Pangaeian precipitation, while perhaps enhancing precipitation at higher tropical latitudes and in equatorial rain shadows. Variability evident in strata with 5th order stratigraphic cycles may have resulted from precipitation changes owing to precession forcing of monsoon circulations and would have differed in character between greenhouse and icehouse climates.

## 1 Introduction

The Earth's climate is in an "icehouse" state. Ice sheets cover Greenland and Antarctica and have, within the last 20 000 yr, covered significant portions of North America, Eurasia, and South America. The last icehouse of comparable duration and intensity to the present one occurred during an interval within the Carboniferous and Permian

CPD

8, 1915–1972, 2012

## Tropical Pangaeian Precipitation

N. G. Heavens et al.

Title Page

Abstract

Introduction

Conclusions

References

Tables

Figures

◀

▶

◀

▶

Back

Close

Full Screen / Esc

Printer-friendly Version

Interactive Discussion



Periods (~330–270 Ma) hereafter termed the Late Paleozoic Ice Age (LPIA). Recognizable glacial facies (diamictites) dating from the LPIA have been identified in sedimentary basins of the former supercontinent Gondwanaland in South America, Africa, Australia, India, Antarctica, and the Arabian Peninsula (Du Toit and Reed, 1927; Fielding et al., 2008).

The LPIA and the late Cenozoic have strong parallels in addition to direct evidence for glaciation. In much of North America and western Europe (tropical Pangaea), LPIA strata are dominated by cyclothem: cyclic successions of interbedded marine and continental strata (commonly including coal) interpreted to reflect high-magnitude glacioeustasy and/or synchronous climate variability (Wanless and Shepard, 1936; Veevers and Powell, 1987; Cecil, 1990; Cecil et al., 2003). Similar successions have been identified in strata of late Cenozoic age (e.g. Carter et al., 1999). Cyclical deposits of eolian siltstone intercalated with paleosols, carbonates, and other facies in the Carboniferous and Permian of western North America may be analogs to late Cenozoic loess and marine dust deposits (e.g. Soreghan et al., 2008a). Some cyclical deposits from the late Paleozoic have spectral characteristics consistent with Milankovitch cycle variations in the Earth's orbit such as the ~100 ka eccentricity cycle (e.g. Schwarzacher, 1989; Birgenheier et al., 2009; Davydov et al., 2010), suggesting that both the late Paleozoic and late Cenozoic icehouses were characterized by high-frequency orbitally-driven variability in glaciation and other aspects of climate. Strong correlations between paleoproxy estimates of  $p\text{CO}_2$ , tropical SSTs, and ice volume on million-year timescales suggest that the late Paleozoic icehouse could have been subject to complex feedbacks involving the cryosphere, biosphere, and hydrosphere similar to those under investigation in the context of late Cenozoic climate (Montañez et al., 2007). The LPIA also was a critical period for biological and ecological evolution, which involved important modern groups such as the amniotes and the haptophytes (Olson, 1966; Sues and Reisz, 1998; Zug et al., 2001; Pough et al., 2008; Liu et al., 2010).

## Tropical Pangaeian Precipitation

N. G. Heavens et al.

[Title Page](#)[Abstract](#)[Introduction](#)[Conclusions](#)[References](#)[Tables](#)[Figures](#)[◀](#)[▶](#)[◀](#)[▶](#)[Back](#)[Close](#)[Full Screen / Esc](#)[Printer-friendly Version](#)[Interactive Discussion](#)

## Tropical Pangaeian Precipitation

N. G. Heavens et al.

Title Page

Abstract

Introduction

Conclusions

References

Tables

Figures

◀

▶

◀

▶

Back

Close

Full Screen / Esc

Printer-friendly Version

Interactive Discussion



The parallels between the climate of the modern world and that of the LPIA have made the latter an attractive target for qualitative climate reconstructions based on geological data (Köppen and Wegener, 1924; Witzke, 1990; Ziegler et al., 1997; Tabor and Poulsen, 2008) and quantitative climate model simulations (Kutzbach and Gallimore, 1989; Crowley et al., 1991; Gibbs et al., 2002; Otto-Bliesner, 2003; Horton et al., 2007, 2010; Poulsen et al., 2007; Peyser and Poulsen, 2008; Horton and Poulsen, 2009). Results of qualitative climate reconstructions suggest that variations in sea level/extent of glaciation strongly correlated with variations in tropical precipitation. The sign of the correlation, however, is disputed. Either the tropics experienced a wetter and less seasonal precipitation regime during glacial (lowstand) intervals than during interglacial (highstand) intervals (glacial humidity: Perlmutter and Matthews, 1989; Cecil et al., 2003; Peyser and Poulsen, 2008; Eros et al., 2012) or a drier and more seasonal precipitation regime during glacial (lowstand) intervals than during interglacial (highstand) intervals (glacial aridity: Soreghan, 1994, 1997; Olszewski and Patzkowsky, 2003; Soreghan et al., 2008a; Falcon-Lang and DiMichele, 2010; Allen et al., 2011).

In addition to the question of glacial-interglacial variability, questions also surround the well-known trend of aridification in tropical Pangaea (e.g. Tabor and Poulsen, 2008). Notable evidence for this trend include the gradual disappearance of the Euramerican coal forests during the Late Carboniferous (e.g. Falcon-Lang and DiMichele, 2010) and increased deposition of evaporites in western tropical Pangaea (e.g. Soreghan et al., 2008a) during the Early Permian. Tabor and Poulsen (2008) thoroughly review possible explanations, including: (1) northward drift of Pangaea; (2) the gradual infill of epeiric seas; (3) increased distance from Paleo-Tethys (a source of moisture) due to the assembly of Pangaea; (4) increased monsoon intensity potentially connected with other factors; (5) variations in central Pangaeian orography; (6) decrease in average ice volume; and (7) higher average  $p\text{CO}_2$ , but were unable to identify any factor as being of “primary importance”.

Previous climate model studies generally support the hypothesis of glacial humidity. The presence of a large ice sheet on Gondwanaland has been shown to inhibit the

summer progress of the Inter-Tropical Convergence Zone (ITCZ) (a zone of high precipitation) into the Southern Hemisphere, though not the Northern Hemisphere (Otto-Bliesner, 2003; Poulsen et al., 2007). A Gondwanan ice sheet suppressing monsoonal circulation over southern tropical Pangaea, however, might have enhanced precipitation over both northern and southern tropical Pangaea. The stronger meridional thermal gradient could have strengthened the Hadley cell in the southern tropics and thus increased the flow of moist air to Pangaea from Paleo-Tethys (Poulsen et al., 2007; Peyser and Poulsen, 2008). Peyser and Poulsen (2008) suggested that this mechanism could explain much of the long-term aridity trend, because aridification appears to have tracked Gondwanan ice sheet retreat (Peyser and Poulsen, 2008).

The purpose of this study is to simulate the glacial-interglacial climate variability evident in the geological record of the LPIA in order to understand its underlying mechanisms. Previous sensitivity studies of this kind have been performed using the GENESIS model (Gibbs et al., 2002; Otto-Bliesner, 2003; Horton et al., 2007, 2010; Poulsen et al., 2007; Peyser and Poulsen, 2008; Horton and Poulsen, 2009). We, however, use the Community Climate System Model version 3 (CCSM3) (Collins et al., 2006; Yeager et al., 2006), a later generation Earth System Model that has been used to simulate Late Permian climate (Kiehl and Shields, 2005) as well as many other aspects of past, present, and future climate. One key advantage of CCSM3 over GENESIS, as acknowledged by Peyser and Poulsen (2008), is that CCSM3 uses a fully prognostic three-dimensional ocean model component rather than a mixed layer ocean model tuned to reproduce modern oceanic heat transport. It, however, takes considerable model time to bring the ocean model component to equilibrium with the atmosphere model component. This equilibration process makes CCSM3 more computationally expensive than older models and therefore limits investigation of dynamic changes in vegetation and glaciation considered in previous studies. However, as described in Sect. 2, we have generated simulations that have relatively stable surface climate and approximate fully equilibrated simulations without fully equilibrating the ocean, thereby allowing a wider suite of experiments than described by Kiehl and Shields (2005).

## Tropical Pangaeian Precipitation

N. G. Heavens et al.

[Title Page](#)[Abstract](#)[Introduction](#)[Conclusions](#)[References](#)[Tables](#)[Figures](#)[◀](#)[▶](#)[◀](#)[▶](#)[Back](#)[Close](#)[Full Screen / Esc](#)[Printer-friendly Version](#)[Interactive Discussion](#)

## 2 Simulations and analysis

### 2.1 The model

All simulations were performed using CCSM3 in a configuration that couples active components that simulate the atmosphere, ocean, land (prescribed vegetation), and sea ice. The atmosphere model has a horizontal resolution of  $3.75^\circ \times 3.75^\circ$  (T31), while the ocean model has 25 layers and a nominal horizontal resolution of  $3^\circ$ . This configuration of CCSM3 is nearly identical to that used by Kiehl and Shields (2005). Yeager et al. (2006) has characterized the biases of this configuration, especially those relative to higher resolution versions of CCSM3.

### 2.2 Paleogeography

The paleogeography used corresponds to the Asselian and Sakmarian Stages of the Permian (299–284 Ma), which began with widespread glaciation, high frequency variability, and low  $p\text{CO}_2$  and ended with a climatic optimum of high  $p\text{CO}_2$  (Isbell et al., 2003a; Montañez et al., 2007). All simulations, except for the control simulations of pre-industrial Late Holocene climate, use basic paleogeographic information appropriate for this era (Appendix A). The ocean grid is the same for all simulations. The advance or retreat of shallow seas by glacioeustatic processes is simulated by representing all areas at altitudes less than 100 m as lakes in the land component of CCSM3 (SL100 configuration) or leaving the land component unmodified in this respect (SL0 configuration).

While converting the information described in Appendix A into model input files, coastlines, seaways, and similar features were modified to prevent the generation of isolated basins (and artificially fresh or saline waters) due to the insufficient resolution of currents (see Rosenbloom et al., 2011, for a more complete discussion). Areas of mismatch between the original land and ocean input information (Appendix A) were

CPD

8, 1915–1972, 2012

## Tropical Pangaeon Precipitation

N. G. Heavens et al.

Title Page

Abstract

Introduction

Conclusions

References

Tables

Figures

◀

▶

◀

▶

Back

Close

Full Screen / Esc

Printer-friendly Version

Interactive Discussion



represented as lakes, since the areas of mismatch likely would have been shallow coastal waters.

### 2.3 Solar, greenhouse gas, and aerosol forcings

All simulations use a fixed solar constant of  $1333 \text{ W m}^{-2}$  (97.5 % of present) in agreement with the model of Gough (1981). Two greenhouse gas scenarios (Table 1), which span the range of  $p\text{CO}_2$  inferred by Montañez et al. (2007), were used. Glacial-interglacial variability in  $p\text{CO}_2$  and  $p\text{CH}_4$  during Plio-Pleistocene time was strongly correlated, so  $p\text{CH}_4$  levels in the greenhouse gas scenarios were adjusted in proportion to  $p\text{CO}_2$  levels according to a linear relation derived from the Vostok ice core data of Petit et al. (1990). Glacial-interglacial variability in  $p\text{N}_2\text{O}$  is certainly evident in the data of Petit et al. (1990) but is less well correlated with  $\text{CO}_2$ , so  $p\text{N}_2\text{O}$  was left at modern levels. While the  $p\text{CH}_4$  in the greenhouse climate scenario (GG2500) may be excessively high, the uncertainties in radiative forcing due to uncertainties in the reconstructed values of  $p\text{CO}_2$  during the Asselian-Sakmarian likely exceed those that arise from uncertainty in the levels of the other greenhouse gases.

Using the first and third equations for  $\text{CO}_2$  and the equation for  $\text{CH}_4$  in Table 6.2 of IPCC (2001), the change in instantaneous radiative forcing between the greenhouse and icehouse greenhouse gas scenarios (GG2500 and GG250) ranges from  $14.1$  to  $16.7 \text{ W m}^{-2}$ , which is equivalent to 3.8 to 4.0 times the radiative forcing due to the doubling of  $\text{CO}_2$  from 385 ppmv to 770 ppmv.

Each simulation uses a prescribed uniform aerosol forcing with a visible optical depth of 0.08, which is lower than that used (0.28) by Kiehl and Shields (2005) and is approximately equal to the pre-industrial “natural” aerosol optical depth estimated by Mahowald et al. (2011). The optical properties of this “background” aerosol are broadly similar to sulfate aerosol.

CPD

8, 1915–1972, 2012

## Tropical Pangaeian Precipitation

N. G. Heavens et al.

Title Page

Abstract

Introduction

Conclusions

References

Tables

Figures

◀

▶

◀

▶

Back

Close

Full Screen / Esc

Printer-friendly Version

Interactive Discussion



## 2.4 Base simulations

Two base simulations (greenhouse.base and icehouse.base) were performed to help create glaciation and vegetation scenarios for the other simulations. Both base simulations used prescribed vegetation consisting of a single biome on land, cool mixed forest, which is a modern mid-latitude biome of qualitatively average characteristics. Each simulation then was run until the trend in the energy imbalance of the model system for the last 100 yr of the run was greater than  $-0.5 \text{ W m}^{-2}$  and the surface temperature trend was within  $\pm 0.05 \text{ K (100 a)}^{-1}$ . In both cases, this process took  $\sim 500$  yr. Our analysis of the simulation output of Kiehl and Shields (2005) suggests a global mean surface temperature bias of  $\sim 0.5^\circ \text{C}$  is introduced by using these criteria rather than the stricter criteria used by Kiehl and Shields (2005). Temperature bias is primarily in polar ocean regions, while precipitation bias is centered on  $30^\circ \text{N}$  and  $30^\circ \text{S}$  over land areas. Bias in both fields near the Equator is much less than the global average, but results there still may be sensitive to the weaker equilibration criteria, as will be discussed in Sect. 4.1. Thirty years of output from the last century of each run then were used to compute climatological means and standard errors of the mean of quantities such as surface temperature and precipitation.

## 2.5 Vegetation

The results of the base simulations, uniform present-day global average soil properties, and appropriate  $p\text{CO}_2$  values were used to force the equilibrium vegetation model BIOME4 (Kaplan et al., 2003). The BIOME4 output was mostly insensitive to the assumed soil properties. The predicted biomes then were converted to equivalent biome types used by the land component of CCSM3 to generate two vegetation scenarios, one for greenhouse climates (V2500), which was generated from the output of the base greenhouse climate simulation (greenhouse.base), and one for icehouse climates (V250), which was generated from the output of the base icehouse climate simulation (icehouse.base) (Fig. 1a and b).

## Tropical Pangaeon Precipitation

N. G. Heavens et al.

Title Page

Abstract

Introduction

Conclusions

References

Tables

Figures



Back

Close

Full Screen / Esc

Printer-friendly Version

Interactive Discussion



## Tropical Pangaeian Precipitation

N. G. Heavens et al.

Title Page

Abstract

Introduction

Conclusions

References

Tables

Figures

◀

▶

◀

▶

Back

Close

Full Screen / Esc

Printer-friendly Version

Interactive Discussion



Note that equilibrium vegetation models such as BIOME4 do not account for processes such as wildfire that strongly affect the modern biome distribution (Bond et al., 2005). Also note that BIOME4 assumes the physiological properties of late Cenozoic vegetation, which likely differ greatly from those of late Paleozoic vegetation (e.g. Wilson and Knoll, 2010). Grassland biomes are retained rather than treated as barren ground, as in Horton et al. (2010), because non-grass plants that were adapted to similar climatic conditions to present-day grasses likely occupied those biomes, though these plants may have been less productive and/or less tolerant of moisture stress than grasses (W. DiMichele, personal communication, 2011).

Percent of possible sunshine is necessary to force BIOME4. To develop the vegetation scenarios, BIOME4 was forced with the ratio between downwelling shortwave radiation at the surface and insolation. This is a physically reasonable estimate of the percent of possible solar radiation incident on a plant but may underestimate percent of possible sunshine, canonically defined as the fraction of hours that a “sunshine recorder” is insufficiently obscured by clouds relative to number of the hours the sun is shining (Hoyt, 1977). Forcing BIOME4 with the additive inverse of total cloudiness, another approximation to percent of possible sunshine canonically defined (Hoyt, 1977), as in Mahowald (2007) produces minor changes in the tropical biome distribution for the greenhouse vegetation scenario (V2500) (and no change elsewhere). For the icehouse vegetation scenario (V250), forcing BIOME4 with the inverse of total cloudiness changes tropical forests/savanna in western equatorial Pangaea, eastern equatorial Pangaea, and South China (the northern landmass in eastern Paleo-Tethys) (Fig. 1b) to xerophytic shrubland.

We did not apply this change to the icehouse vegetation scenario (V250), because widespread replacement of tropical forests by xeric shrublands in equatorial Pangaea post-dates the Asselian Stage, our target interval. Late Carboniferous (Gzhelian) floras of Illinois are similar to Late Carboniferous (Gzhelian) and Early Permian (Asselian) floras of France (Galtier, 2008), suggesting that the classical lowland/wetland/coal forest flora of Late Pennsylvanian Euramerica survived into the Asselian in eastern equatorial

Pangaea. Moreover, the earliest-known appearance of a dominantly xeric flora in low-land tropical western equatorial Pangaea is from the Kungurian Stage (DiMichele et al., 2001). If the floral transition occurred during the Asselian itself, the simulations that use the icehouse vegetation scenario may be biased warmer and wetter, particularly in the tropics.

When implemented in CCSM3, the phenology of leaf area index and stem area index etc. are prescribed by using the biome mean under present-day conditions. Note that present-day biomes of the same type can have diverse phenological and other properties.

## 2.6 Glaciation

Two polar glacial configurations (ICES and ICEB) were developed. First, the mean daily liquid equivalent snow depth climatology of the icehouse climate base simulation (icehouse.base) was used to generate potential distributions of land ice. Second, a network algorithm was used to assemble potential land ice areas into discrete ice sheets. The volume/height of the ice sheet were parameterized using the formulas given in Isbell et al. (2003b). Third, the algorithm was tuned to generate a desired sea level change/land ice distribution (Table 2).

The glacial configurations are used to prescribe the locations of land ice in CCSM3. Land ice overrides the original vegetation and its altitude is arithmetically added to the topographic basemaps. An error in the implementation of the glacial configuration design algorithm discovered after completion of the model experiments gave land ice ~30 % higher altitude than intended (3500 m vs. 2700 m for the big polar glacial configuration, ICEB). CCSM3 simulations of the Last Glacial Maximum suggest that ice sheet topography can have significant effects on polar and mid-latitude circulation patterns in the hemisphere of the ice sheet, so this error is not trivial (Otto-Bliesner et al., 2006). However, this error is of comparable importance to the error introduced by prescribing uniform topography across an individual ice sheet. Moreover, the maximum altitudes of the ice sheets are similar to the predictions of ice sheet model simulations

CPD

8, 1915–1972, 2012

## Tropical Pangaeian Precipitation

N. G. Heavens et al.

Title Page

Abstract

Introduction

Conclusions

References

Tables

Figures

◀

▶

◀

▶

Back

Close

Full Screen / Esc

Printer-friendly Version

Interactive Discussion



for late Paleozoic conditions (Soreghan et al., 2008b) as well as late Cenozoic ice sheets (Lythe and Vaughan, 2001). In any case, caution should be exercised when estimating regional variability in the vicinity of the Gondwanan ice sheets from these simulations.

5 The small and big polar glacial configurations (ICES and ICEB) are meant to represent the relatively small Gondwanan ice sheets proposed by Isbell et al. (2003a, b) and supported by a recent re-assignment of glacial deposits in Saudi Arabia to higher paleo-latitude (Melvin et al., 2010). In both configurations (Fig. 1c and d), land ice is minimal in Gondwanaland at  $\sim 240^\circ$  longitude, which corresponds to Antarctica, where  
10 the presence of a large ice sheet has been disputed (Isbell et al., 2003a). This minimum arises directly from a minimum in snowfall, which is robust feature of late Paleozoic simulations in CCSM3 generally, including those of Kiehl and Shields (2005). This snowfall minimum is associated with a semi-permanent high-pressure center in spring and fall, an obvious limiting factor for snowfall. The absence of ice sheets in late Cenozoic eastern Siberia long has been attributed to similar causes (e.g. Gerasimov and Markov,  
15 1939).

A small patch of land ice is present in Angara (the northern continent). There is disputed evidence for glaciation in Angara (present-day Siberia) during the Permian (see discussion by Shi and Waterhouse, 2010), but it is included in these configurations  
20 for consistency rather than as an interpretation of extant geological evidence.

A third glacial configuration (ICEH) explores an extreme, but geologically plausible scenario. Proglacial and periglacial facies have been hypothesized in tropical Pangaea at paleo-altitudes as low as  $\sim 500\text{--}1000\text{ m}$  (Becq-Giraudon et al., 1996; Sweet and Soreghan, 2008; Soreghan et al., 2008a, b, 2009). It is difficult to explain how mountain glaciation could flourish near the Equator while ice sheets remained relatively small, and climate model simulations confirm the difficulty (Soreghan et al., 2008b). The huge glacial configuration (ICEH) uses the results of an icehouse simulation forced by the big polar glacial configuration (icehouse.glaciation.big) (Table 3) to calculate the maximum seasonal mean  
25

## Tropical Pangaeian Precipitation

N. G. Heavens et al.

Title Page

Abstract

Introduction

Conclusions

References

Tables

Figures



Back

Close

Full Screen / Esc

Printer-friendly Version

Interactive Discussion



temperature, denoted December-January-February (DJF), March-April-May (MAM), June-July-August (JJA), September-October-November (SON); at the paleo-location of the proglacial/periglacial facies identified by Soreghan et al. (2009). Land ice was then imposed at all areas whose highest seasonal mean temperature was lower than this temperature (25.6 °C). Topography was left unmodified. Key details of each configuration are given in Table 2.

## 2.7 Simulations after base simulations

Various simulations besides the base simulations were performed, brought to equilibrium, and evaluated as described in Sect. 2.4. In addition, 100-yr hybrid simulations were run to test the sensitivity of some of these simulations to changes in orbital parameters. Note that in all simulations, the solstices and equinoxes occur on the same day of year they would in a present day simulation. To provide a context for the simulations relative to modern climate, two late Holocene pre-industrial control simulations (pic1 and pic2), which met the equilibration criteria in Sect. 2.4, were performed. These simulations only differ in their vegetation prescriptions and meet the same criteria used to evaluate the stability of the design simulations. A full list of the late Paleozoic climate simulations and their configurations are given in Table 3.

## 3 Results

### 3.1 Overview

Global mean temperature and precipitation (Fig. 2a and e), as well as the spatial distribution of annual mean temperature and precipitation (Figs. 3–5) are consistent with expected patterns. Annual mean surface temperature isotherms are mostly zonally symmetric, but they bend equatorward toward the mid-latitude coastlines of Pangaea and the northern coast of Angara (Fig. 3b–d). The bending of isotherms in these areas reflects the combined effects of coastal land areas remaining cooler than the ocean

## Tropical Pangaeian Precipitation

N. G. Heavens et al.

Title Page

Abstract

Introduction

Conclusions

References

Tables

Figures

◀

▶

◀

▶

Back

Close

Full Screen / Esc

Printer-friendly Version

Interactive Discussion



5 during the winter (owing to the lower thermal inertia of land and snow albedo effects), and remaining cooler than the continental interior during summer (owing to land-sea breeze interactions). The Central Pangaeian Mountains (CPM) are also cooler than other areas at the same latitude. The tropics are generally wetter than the sub-tropics, and tropical Pangaea is generally drier than tropical ocean areas (Fig. 4a–d). Like the present-day equatorial western Pacific Ocean, the equatorial western Panthalassic Ocean is unusually cool and dry due to strong upwelling of cold waters from the deeper ocean and the resulting inhibition of tropical convection (Figs. 3b–d, 4 and 5). These patterns are apparent in the simulations of Kutzbach and Ziegler (1993) and Peyser and Poulsen (2008), though the extent of Panthalassic equatorial upwelling is greater in the present study than in those past simulations.

10 Most importantly, mean tropical temperatures in more glaciated simulations (the icehouse.glaciation.big and icehouse.glaciation.huge series) bracket the 2 s.e. (standard error of the mean) interval for the Middle Pennsylvanian tropical temperature anomaly relative to present climate (pic simulations) based on clumped isotope thermometry (Came et al., 2007) (Fig. 2d). These simulations thus encompass a good estimate of the potential range of LPIA climates.

15 Global mean characteristics divide the late Paleozoic climate simulations into three groups (Fig. 2 and Table 4). The greenhouse climate simulations (Fig. 2, Cases 1, 3–6) and the less glaciated icehouse climate simulations (Fig. 2, Cases 2, 7–16) mainly differ due to the variability in  $p\text{CO}_2$  and  $p\text{CH}_4$  levels between the groups (see Table 4 for complete case numbering). Differences between the base simulations (greenhouse.base and icehouse.base) may not capture the fullness of this effect due to the concurrent effect of the differential use of the sea level (SL) configurations. This latter effect is approximately the difference between the unglaciated icehouse scenario with high sea level and the one with low sea level (icehouse.highsealevel and icehouse.noglaciation).  
20 When this correction is applied, the change in global annual mean surface temperature attributable to using the higher-level greenhouse gas scenario (GG2500) rather than the lower-level greenhouse gas scenario (G250) is 9.1 °C. Thus, the sensitivity of

## Tropical Pangaeian Precipitation

N. G. Heavens et al.

[Title Page](#)[Abstract](#)[Introduction](#)[Conclusions](#)[References](#)[Tables](#)[Figures](#)[Back](#)[Close](#)[Full Screen / Esc](#)[Printer-friendly Version](#)[Interactive Discussion](#)

surface temperature to a doubling of CO<sub>2</sub> is 2.3 to 2.4 °C, which brackets the equilibrium sensitivity of CCSM3's T31 configuration, 2.32 °C, estimated by Kiehl et al. (2006).

Land ice in less glaciated simulations (glaciation.small and glaciation.big) primarily lowers land temperatures, particularly at the location of the land ice (Fig. 2b, Cases 11 and 12 vs. Case 8, Case 6 vs. Case 3; cf. Figs. 1c and 3c). As ice sheets grow, their effects become more global. The simulations that use the huge ice configuration (icehouse.glaciation.huge and its hybrids) have far more land ice than the other simulations, particularly in upland and mountain areas near the Equator (Table 2, Fig. 1c). These simulations therefore would be expected to comprise a third distinct group. However, ocean temperatures in these simulations are ~10 °C cooler and sea ice area is around four times greater than in less glaciated simulations (Fig. 2c, Table 4).

Vegetation, as inferred from the contrast between unglaciated and base simulations (.noglaciation and .base), cools both ocean and land (Fig. 2b and c, Case 3 vs. Case 1 and Case 8 vs. Case 2). The cooling effect of vegetation stronger in the icehouse simulations than the greenhouse simulations, possibly due to the greater expanse of bright, subtropical deserts in the icehouse vegetation scenario (V250) (Fig. 1a and b) or other differential changes relating to albedo. The first pre-industrial control simulation (pic1) is warmer than the second one (pic2), particularly over land (Fig. 2b, Case 20 vs. Case 21). The first pre-industrial control simulation uses BIOME4 and the mean biome properties in its vegetation prescription, just like the late Paleozoic simulations, suggesting that the approach used to prescribe vegetation in the late Paleozoic simulations may introduce a similar temperature bias.

Higher sea level lowers surface temperatures, particularly on land (Fig. 2b, Case 7 vs. Case 8). At the global scale, variability among the orbital sensitivity simulations and the simulations from which they are hybridized is generally similar to the estimated systematic bias due to the equilibration criteria (e.g. Fig. 2a, Cases 12–16). The simulations that use the huge glacial configuration (ICEH) are exceptions (Fig. 2a, Cases 17–19). Global mean surface temperature in these simulations can vary up to 2.6 °C due to orbital variability, an order of magnitude greater than in the other orbital

## Tropical Pangaeon Precipitation

N. G. Heavens et al.

Title Page

Abstract

Introduction

Conclusions

References

Tables

Figures

◀

▶

◀

▶

Back

Close

Full Screen / Esc

Printer-friendly Version

Interactive Discussion



sensitivity simulations (Table 4). That this behavior appears in the coldest simulations suggests that these changes may be due to a strong response of sea ice (the most dynamic aspect of the cryosphere) to changes in insolation.

Northern Hemisphere sea ice cover (% of all area at a given latitude with sea ice) in these simulations indeed is strongly controlled by summer insolation. The simulation with weakest northern summer insolation (ih.g.h.ecc) has greater Northern Hemisphere sea ice cover than the other simulations in both northern summer (Fig. 6a, “cold NH summer”) and northern winter (Fig. 6b, “cold NH winter”), while Southern Hemisphere sea ice cover is unaffected (Fig. 6a and b). Sea ice variability is also strongly sensitive to insolation in the simulations that use smaller glacial configurations. Yet in less glaciated simulations, sea ice variability has a limited effect on global climate; sea ice covers less proportional area and is confined to higher latitudes, where there is less area and insolation relative to the rest of the globe (Fig. 6c and d).

To first order, global precipitation strongly correlates with surface temperature ( $r = 0.99$ ). Referenced to the pre-industrial control run with prescribed observed vegetation (pic2), the linear slope of this relation (the sensitivity of global precipitation to surface temperature change) is  $2.1\% \text{ } ^\circ\text{C}^{-1}$ , consistent with global simulations of modern climate (including ones using CCSM3) analyzed by Held and Soden (2006). This relationship, however, does not necessarily govern partitioning of precipitation between land and ocean. For instance, the unglaciated icehouse simulation with high sea level (icehouse.highsealevel) is significantly cooler than the equivalent simulation with low sea level (icehouse.noglaciation), both globally (Fig. 2a, Cases 7 and 8) and over land (Fig. 2b, Cases 7 and 8), but is significantly wetter over land (Fig. 2f, Cases 7 and 8).

Geography also affects precipitation and temperature. The pre-industrial control simulations (pic1 and pic2) have global mean surface temperatures similar to the less glaciated icehouse simulations (icehouse.highsealevel, icehouse.noglaciation, icehouse.glaciation.small, and icehouse.glaciation.big), but the pre-industrial control simulations are significantly wetter over land, a demonstration of the strong continentality of late Paleozoic geography (Kutzbach and Gallimore, 1989) (Fig. 2f, Cases 20 and 21

## Tropical Pangaeon Precipitation

N. G. Heavens et al.

Title Page

Abstract

Introduction

Conclusions

References

Tables

Figures



Back

Close

Full Screen / Esc

Printer-friendly Version

Interactive Discussion



vs. Cases 7–16). This strong continentality is reproduced in the mean temperature and precipitation fields (Figs. 3 and 4).

Land ice generally has a drying effect, evident locally (Fig. 4b–d) and globally through the feedbacks that set the global temperature-precipitation relation (e.g. Fig. 2e, Case 8 vs. Cases 11, Case 12, and Case 17), but there is an important exception. In most of the simulations, the model successfully resolves a rain shadow between the Ancestral Rocky Mountains and the Alleghanian orogenic belt ( $\sim 5^\circ$  N,  $160^\circ$ , approximately modern Iowa, Illinois, and Minnesota) that strongly contrasts with warm and wet conditions throughout the Central Pangaeon Mountains (CPM) (Fig. 4a–c). However, this rain shadow mostly disappears (Fig. 4d) when significant land ice is placed on the CPM. The glaciated CPM becomes arid, while areas to the north and south, including the former rain shadow become wetter.

Note, however, that the huge glacial configuration (ICEH) is not consistent with the resulting climate. Annual mean temperatures over the CPM are only  $< 0^\circ$  C over its highest peaks ( $0^\circ$  N,  $170^\circ$ ) (Fig. 3d). Summer (JJA for most of the CPM) temperatures are even more unfavorable. Lower greenhouse gas levels, higher aerosol loading, or some other negative radiative forcing would be necessary to keep land ice stable over the CPM (or on the islands on the western side of Paleo-Tethys), as also found by Soreghan et al. (2008b).

Orbital forcing, too, can affect low-latitude Pangaeon precipitation, particularly the extent and aridity of the sub-tropical deserts (Fig. 5a–d). The longitude of perihelion has a stronger effect than obliquity (that is, the effect is stronger when comparing the left and right set of panels in Fig. 5 as opposed to comparing the top and bottom set), suggesting summer insolation is driving tropical precipitation. Near the equator and close to the sub-tropics, the seasonality of precipitation is consistent between the orbital forcing simulations in Fig. 5. Precipitation peaks in summer and fall and is lowest in winter (Fig. 7). Even at  $5^\circ$  N, relatively wet for most of the year, DJF precipitation averages no more than 30 mm (Fig. 7a). Depending on hemisphere and latitude, the spring can be drier or wetter (Fig. 7b and d). Orbital forcing primarily affects summer

## Tropical Pangaeon Precipitation

N. G. Heavens et al.

[Title Page](#)[Abstract](#)[Introduction](#)[Conclusions](#)[References](#)[Tables](#)[Figures](#)[◀](#)[▶](#)[◀](#)[▶](#)[Back](#)[Close](#)[Full Screen / Esc](#)[Printer-friendly Version](#)[Interactive Discussion](#)

precipitation in the sub-tropics (Fig. 7a and c), but equatorial precipitation increases in the summer hemisphere and decreases in the winter hemisphere in simulations with perihelion at summer solstice (e.g. Fig. 7c). This seasonality of precipitation and the enhancement of precipitation under higher summer insolation is indicative of a monsoonal climate, whose dynamics will be investigated in Sect. 3.2.

### 3.2 Monsoonal variability

A monsoon is a seasonally reversing wind system. In general, we will speak of its behavior and intensity in the summer hemisphere, where a typical monsoon displaces the ITCZ poleward in a narrow longitudinal band, resulting in higher precipitation in some areas closer to the summer hemisphere tropic. The late Cenozoic South Asian Monsoon is associated with a strong cross-equatorial westerly jet at ~1500 m above the surface (Bunker, 1965; Joseph and Sijikumar, 1998; Webster and Fasullo, 2003). This feature is apparent, if poorly resolved, in climate models and re-analysis data, so the difference in zonal wind velocity in the lower troposphere (850 hPa) between the equator and the summer hemisphere tropic is a good proxy for monsoon intensity (Wang et al., 2001).

Seasonally reversing wind systems that resemble the South Asian Monsoon are present in the late Paleozoic climate simulations (Fig. 8). In the ordinary greenhouse simulation (greenhouse.noglaciation), a Pangaeen monsoon is apparent in both hemispheres (Fig. 8a and e), which marks this monsoon as the classic “megamonsoon” of Kutzbach and Gallimore (1989). The monsoon jet is much less apparent in the analogous icehouse simulation (icehouse.noglaciation) (Fig. 8b and f). A potentially distinct megamonsoon is apparent over Paleo-Tethys in both simulations.

A simple monsoon circulation index (analogous to those presented by Wang et al., 2001) was defined for Pangaea and calculated. Monsoon intensity generally is stronger in the high greenhouse gas than the low greenhouse gas simulations (Fig. 9a and b). Changing orbital forcing can significantly enhance or diminish monsoon intensity (e.g. Fig. 9a and b, icehouse.noglaciation vs. ih.ng.ecc and ih.ng.ecc4).

## Tropical Pangaeen Precipitation

N. G. Heavens et al.

Title Page

Abstract

Introduction

Conclusions

References

Tables

Figures



Back

Close

Full Screen / Esc

Printer-friendly Version

Interactive Discussion



## Tropical Pangaeon Precipitation

N. G. Heavens et al.

Title Page

Abstract

Introduction

Conclusions

References

Tables

Figures

◀

▶

◀

▶

Back

Close

Full Screen / Esc

Printer-friendly Version

Interactive Discussion



High summer insolation strengthens the monsoon, while low summer insolation suppresses it (Fig. 9a, ih.g.h.ecc vs. ih.g.h.ecc4, ih.g.b.ecc2 vs. ih.g.b.ecc, ih.g.b.ecc3 vs. ih.g.b.ecc4, ih.ng.ecc vs. ih.ng.ecc4, gh.ng.ecc4 vs. gh.ng.ecc). These orbitally forced monsoons are not megamonsoons, since the Northern Hemisphere monsoon will be strong under the same conditions that a Southern Hemisphere monsoon is suppressed and vice versa. The presence of ice sheets (Fig. 9a, icehouse.glaciation.huge vs. icehouse.glaciation), greenhouse gas levels (Fig. 9a, greenhouse.base vs. icehouse.base), and the vegetation distribution (Fig. 9a and b, icehouse.base vs. icehouse.noglaciation) potentially set background monsoon intensity. Orbital forcing is less effective at suppressing the monsoon under high greenhouse gas levels (Fig. 9a, gh.ng.ecc; Fig. 9b, gh.ng.ecc4 vs. ih.g.h.ecc4, ih.g.b.ecc4, and ih.ng.ecc4).

The monsoon circulation indices correlate significantly with annual precipitation at 20° N and 20° S (Fig. 9c and d), especially if the simulations that use the huge glacial configuration (icehouse.glaciation.huge and its hybrids) are excluded as outliers. Exclusion is justified, because precipitation in these simulations at 20° N and 20° S is an order of magnitude greater than simulations with comparably weak monsoons (Fig. 9c and d). In addition, we previously noted in Sect. 3.1 that the precipitation regime in a rain shadow area in west-central equatorial Pangaea radically changes in these simulations. Therefore, some mechanism in these simulations is producing monsoon-like precipitation patterns in the absence of a classical monsoonal circulation (see discussion in Sect. 3.3). Thus, while other processes may be important, especially when there is tropical glaciation, changes in monsoonal intensity appear to be the leading control on tropical Pangaeon precipitation. A stronger monsoon spreads the ITCZ over the northern tropics, while a weaker monsoon focuses it near the Equator. This effect can be illustrated by meridional streamfunction analysis over Pangaea, in which the monsoon manifests as a seasonally varying cross-equatorial meridional cell (Fig. 10a–d).

The monsoonal circulation over Paleo-Tethys and the western Panthalassic Ocean (Fig. 11) (hereafter the Paleo-Tethyan monsoon) is more difficult to suppress than the Pangaeon monsoon and strengthens under low greenhouse gas levels (Fig. 11a

and b, contrast icehouse simulations and greenhouse simulations). Its response to orbital forcing differs from that of the Pangaeian monsoon. The Paleo-Tethyan monsoon is often weakened rather than strengthened by strong summer insolation (Fig. 11a, ih.ng.ecc4 vs. ih.ng.ecc3, gh.ng.ecc4 vs. gh.ng.ecc3; Fig. 11b, ih.g.b.ecc3 vs. ih.g.b.ecc4, ih.g.b.ecc vs. ih.g.b.ecc2, ih.ng.ecc vs. ih.ng.ecc4, gh.ng.ecc vs. gh.ng.ecc4), and so its intensity is anti-correlated with that of the Pangaeian monsoon ( $r = -0.80$ ,  $p < 10^{-4}$ ). Excluding the most glaciated (lowstand.glaciation.huge and its hybrids) simulations, Paleo-Tethyan monsoon intensity is anti-correlated with subtropical precipitation, particularly over South China (Fig. 11c and d). Yet glaciation of the CPM does not appear to affect the precipitation regime over Paleo-Tethys; the simulations that include it (lowstand.glaciation.huge and its hybrids) do not appear to be outliers. These simulations are excluded from the correlation analysis for the sake of consistency with the Pangaeian monsoon analysis.

### 3.3 The tropical circulation and precipitation regime under deep icehouse conditions

As discussed in Sect. 3.1, the precipitation regime and tropical Pangaeian atmospheric circulation in the most glaciated simulations (icehouse.glaciation.huge and its hybrids) are somewhat different than in the other simulations. In particular, annual mean precipitation near each tropic is similar to annual mean precipitation when the monsoon is strong (Figs. 4d, 9c and d), yet the monsoon is weak (Fig. 9a and b). Winds at 850 hPa at  $\sim 15^\circ$  latitude in the summer hemisphere are westerly in strong monsoon simulations (Fig. 12a, b, e and g) and strongly easterly in weak monsoon simulations (Fig. 12c and f). Yet when the CPM is glaciated, strong meridional winds emerging from the CPM dominate weak easterly zonal wind flow at  $15^\circ$  (Fig. 12d and h). These winds appear to drive the equatorial band of heavy rainfall farther into the summer hemisphere (Fig. 12d and h). Consistent with this explanation, the summer hemisphere tropical meridional overturning cell over Pangaea is located farther poleward and/or is stronger than in less glaciated simulations with suppressed monsoons (cf. Fig. 13a, b, c and d).

## Tropical Pangaeian Precipitation

N. G. Heavens et al.

[Title Page](#)[Abstract](#)[Introduction](#)[Conclusions](#)[References](#)[Tables](#)[Figures](#)[◀](#)[▶](#)[◀](#)[▶](#)[Back](#)[Close](#)[Full Screen / Esc](#)[Printer-friendly Version](#)[Interactive Discussion](#)

## 4 Discussion

### 4.1 The changing of the monsoons

Changes in the Pangaeian monsoon drive tropical precipitation variability within most of the model simulations. In the classical view, a monsoon is a large sea/land breeze system (Stanley, 1999; Webster and Fasullo, 2003). Land has a lower thermal inertia than the ocean, so a large landmass bordering the ocean is warmer than the ocean during the summer and colder during the winter. Ascent of warm air heated by the land thus generates low pressure (relative to the ocean) over the land during the summer. The reverse mechanism generates high pressure in the winter, creating a pressure gradient that supports a seasonally reversing wind regime. Two important modifications to this simple portrait have been proposed. First, land-sea contrast may be irrelevant. A sufficiently strong meridional gradient in sea surface temperature can produce a robust monsoon by similar mechanisms to a monsoon based on land-sea contrast (Chao and Chen, 2001). Second, the cross-equatorial circulation of a monsoon is most responsive to thermal forcing when the tropical circulation intrinsically conserves angular momentum rather than deriving it from large-scale eddies elsewhere (Bordoni and Schneider, 2008). Thus, extratropical eddies, which exchange angular momentum and heat with the tropics, can have significant effects on the intensity of a monsoonal circulation and the timing of its initiation (Bordoni and Schneider, 2008; Boos and Kuang, 2010). A monsoon's success thus may be dependent on its insulation from extratropical influence. Possible extratropical influences on the monsoon therefore are the most likely way that the major results of this study could be affected by systematic biases due to the limited equilibration of the model (Sect. 2.4) or unrealistic ice sheet topography (Sect. 2.6).

Variations in greenhouse gas levels and the Earth's orbit during late Paleozoic time could have driven changes in the intensity of two monsoonal circulations, one over Pangaea and the other over Paleo-Tethys (Figs. 9 and 11). At low greenhouse gas levels, the Pangaeian monsoon would have been relatively weak but could be activated in a

## Tropical Pangaeian Precipitation

N. G. Heavens et al.

Title Page

Abstract

Introduction

Conclusions

References

Tables

Figures



Back

Close

Full Screen / Esc

Printer-friendly Version

Interactive Discussion



single hemisphere (and suppressed in the opposite hemisphere) by increased summer insolation (a consequence of high eccentricity and summer longitude of perihelion). High summer insolation, in turn, would strengthen cross-equatorial thermal contrast between the sub-tropics as well as land-ocean thermal contrast in the summer hemisphere. This effect has been widely simulated in late Cenozoic climate (see discussion by Kutzbach et al., 2008), though observations suggest ice sheet dynamics introduce important secondary feedbacks through meltwater export to the ocean (Cheng et al., 2009).

Ice sheets, particularly larger ones, seem to reduce the background intensity of the Pangaean monsoon, but even the largest glacial configuration used in this study (ICEH) is insufficient to suppress the effects of summer insolation forcing (Fig. 9a and b, ih.g.h.ecc and ih.g.h.ecc4). Previous modeling suggested that larger ice sheets weaken the Southern Hemisphere monsoon but not the Northern Hemisphere monsoon (Peyser and Poulsen, 2008), but these simulations do not support this idea. The largest glacial configuration of Peyser and Poulsen (2008) only had land ice in the Southern Hemisphere, whereas the largest ice sheet configuration in this study (ICEH) has a substantial Northern Hemisphere ice sheet in Angara (Fig. 1c). It is thus possible that a large ice sheet is capable of suppressing the monsoon only in its own hemisphere, perhaps through changes in the extratropical forcing.

The Pangaean monsoon intensifies at higher greenhouse gas levels but remains responsive to summer insolation forcing, reducing the intensity of the megamonsoon in the cold summer hemisphere (Fig. 8a and b). The intensification of the Pangaean monsoon under elevated greenhouse gas levels has been simulated before (Peyser and Poulsen, 2008) but is not understood. One possible explanation is that greenhouse warming will tend to strengthen monsoon circulations based on land-sea contrasts, since greenhouse warming is stronger over land than the ocean (Meehl and Arblaster, 2003). The mean land-sea temperature difference in simulations with higher greenhouse gas levels is greater than in simulations with lower greenhouse gas levels (Table 4, greenhouse vs. icehouse). In the former case, annual average sub-tropical

CPD

8, 1915–1972, 2012

## Tropical Pangaean Precipitation

N. G. Heavens et al.

Title Page

Abstract

Introduction

Conclusions

References

Tables

Figures

◀

▶

◀

▶

Back

Close

Full Screen / Esc

Printer-friendly Version

Interactive Discussion



temperatures over Pangaea exceed those in the “tropical warm pool” of the western Panthalassic; in the latter case, temperatures in the two regions are similar (cf. Fig. 3a with Fig. 3c and d).

The Paleo-Tethyan monsoon has limited effects on precipitation over Paleo-Tethys, let alone tropical Pangaea. It is thus no surprise that Paleo-Tethyan monsoons have been simulated before (Fig. 3 of Kutzbach and Ziegler, 1993; Kiehl and Shields, 2005, Fig. 14 of this study) but have not been discussed. The Paleo-Tethyan monsoon may be driven by sea surface temperature contrast between the western and eastern end of Paleo-Tethys (Chao and Chen, 2001; Kiehl and Shields, 2005), but the dynamics of its response to insolation forcing are unclear.

## 4.2 The consequences of CPM glaciation

In the most glaciated simulations (icehouse.glaciation.huge and its hybrids), glaciation of the CPM suppresses precipitation over the CPM but generates strong winds that flow from the CPM into the summer hemisphere. These winds displace the ITCZ poleward, enhancing subtropical precipitation, even when the monsoonal circulation is weak.

We think it most likely that the circulation responsible for this phenomenon, like the monsoonal circulation, is driven by large-scale thermal contrast. In this case, however, the contrast is not between the winter and summer sub-tropics but between the cold, glaciated CPM and the strongly heated non-glaciated land surface near the summer hemisphere tropic. This circulation is confined to a single hemisphere, since the glaciated CPM is located at the Equator. If this explanation is correct, the glaciated CPM, if displaced to the south of the Equator (as in Pennsylvanian time), would enhance the thermal forcing driving the Northern Hemisphere monsoonal circulation and weaken the thermal forcing driving the Southern Hemisphere monsoonal circulation. The ensemble of simulations does not allow us to address readily the contribution of the Angaran and Gondwanan ice sheets to these changes in the tropical circulation and precipitation.

CPD

8, 1915–1972, 2012

## Tropical Pangaeian Precipitation

N. G. Heavens et al.

Title Page

Abstract

Introduction

Conclusions

References

Tables

Figures

◀

▶

◀

▶

Back

Close

Full Screen / Esc

Printer-friendly Version

Interactive Discussion



### 4.3 Glacial aridity or glacial humidity?

Even given a perfect model, glacial-interglacial variability in precipitation in late Paleozoic Pangaea would be difficult to determine. Even if the observational constraints on the problem (sedimentological, paleontological, and geochemical proxies) were precisely known and accurately interpreted, the inputs (greenhouse gas levels, paleogeography, extent of glaciation etc.) are not well constrained. The simulations are grounded in reasonable guesses about these uncertain inputs. They span the tropical temperature anomaly for the Middle Pennsylvanian estimated by Came et al. (2007) and also some warmer climates. Yet they test sensitivities within plausible forcing scenarios; they are not valid simulations of the climate at given instants of time.

Therefore, we will use the simulations to estimate the sensitivity of precipitation ( $P$ ) to each studied climate forcing. As discussed in Sect. 3.1, the change in precipitation due to the difference between the high greenhouse gas level scenario (GG2500) and the low greenhouse gas level scenario (GG250) can be estimated from differencing the base simulations and subtracting the difference between the two unglaciated icehouse simulations (icehouse.highsealevel and icehouse.noglaciation). We then normalize by the equivalent doublings of  $\text{CO}_2$  (Sect. 2.3) to obtain in units of ( $\text{mm doubling}^{-1}$ ):

$$F_{\text{GG}} = \frac{\Delta P}{\Delta(2 \times p\text{CO}_{2\text{eq}})} = \frac{P(\text{greenhouse.base}) - P(\text{icehouse.base}) + P(\text{icehouse.noglaciation}) - P(\text{icehouse.highsealevel})}{3.9} \quad (1)$$

Similar arguments can be used to derive sensitivities for sea level (Sect. 2.2) in units of ( $\text{mm m}^{-1}$ ):

$$F_{\text{SL}} = \frac{P(\text{icehouse.highsealevel}) - P(\text{icehouse.noglaciation})}{100} \quad (2)$$

For glaciation, we calculate sensitivities based on two glacial scenarios to account for the potential non-linear effects of a glacial configuration with significant equatorial land

CPD

8, 1915–1972, 2012

## Tropical Pangaeon Precipitation

N. G. Heavens et al.

Title Page

Abstract

Introduction

Conclusions

References

Tables

Figures

◀

▶

◀

▶

Back

Close

Full Screen / Esc

Printer-friendly Version

Interactive Discussion



ice (ICEH) relative to one in which glaciation is confined close to the poles (ICEB). The units are  $(\text{mm} \times (10^6 \text{ km}^2)^{-1})$  (see Sect. 2.6 and Table 2 for further details).

$$F_{\text{ICEB}} = \frac{P(\text{icehouse.glaciation.big}) - P(\text{icehouse.vegetation})}{17}, \quad (3)$$

$$F_{\text{ICEH}} = \frac{P(\text{icehouse.glaciation.huge}) - P(\text{icehouse.glaciation.big})}{(79 - 17)}$$

We treat the effects of obliquity as independent of eccentricity and longitude of perihelion. The sensitivity is evaluated for a simulation with only high-latitude land ice (lowstand.glaciation.big) to avoid the complexities introduced by CPM glaciation (see Table 3 for details).

$$F_{\theta} = \frac{P(\text{ih.g.b.ecc4}) + P(\text{ih.g.b.ecc3}) - P(\text{ih.g.b.ecc2}) - P(\text{ih.g.b.ecc})}{2(25 - 22)} \quad (4)$$

The units of  $F_{\theta}$  are  $\text{mm degree}^{-1}$ .

The joint sensitivity due to eccentricity ( $\varepsilon$ ) and longitude of perihelion ( $\lambda$ ) is then:

$$F_{\varepsilon\lambda} = \frac{P(\text{ih.g.b.ecc4}) + P(\text{ih.g.b.ecc2}) - P(\text{ih.g.b.ecc3}) - P(\text{ih.g.b.ecc})}{2 \cdot 0.057}, \quad (5)$$

which is the expected amplitude in precipitation in mm during a precession cycle per unit eccentricity, or in a strict sense:  $\Delta P / \Delta (\varepsilon \sin \lambda)$  (see Table 3 for details).

The sensitivity patterns (Fig. 15a–f) match the less comprehensive presentation in Sect. 3. Forcings immediate to the tropics (sea level and tropical glaciation) dominate rather than high-latitude glaciation. If the CPM were not glaciated, equatorial Pangaea would remain quite humid (Fig. 4a–c). The effect of changes in greenhouse gases are harder to assess. The difference in atmospheric  $\text{CO}_2$  and  $\text{CH}_4$  between the Last Glacial Maximum and the pre-industrial Late Holocene is equivalent to  $\sim -0.6$  doublings of  $\text{CO}_2$ , whereas the sea level difference is  $\sim 120$  m (Petit et al., 1990; IPCC, 2001; Fairbanks, 1989). For this amplitude of variability, the effect of sea level change would dominate the effect of greenhouse gas change (Fig. 16). However, when examining precipitation change during the inferred Sakmarian deglaciation (Moñtanez et

## Tropical Pangaeian Precipitation

N. G. Heavens et al.

Title Page

Abstract

Introduction

Conclusions

References

Tables

Figures

◀

▶

◀

▶

Back

Close

Full Screen / Esc

Printer-friendly Version

Interactive Discussion



al., 2007) or a potentially higher amplitude of precession/eccentricity cycle greenhouse gas variability (Horton and Poulsen, 2009), the reverse may be true.

We rely on current understanding of the connection between orbital forcing and late Cenozoic glaciation to interpret the orbital parameter sensitivities. In one view, major expansions and contractions of ice sheets are tuned to the eccentricity cycles (Cheng et al., 2009). Ice sheets gradually expand near the minima of eccentricity cycles due to the weakness of precession forcing. As eccentricity increases, expansion is swift when aphelion occurs during southern summer. Yet the ice sheet ablates quickly when perihelion is during southern summer and then more gradually as eccentricity decreases once more.

Such a scenario may explain Pennsylvanian glacial humidity in the Donets Basin (far eastern equatorial Pangaea) inferred by Eros et al. (2012). Precipitation in this region is relatively insensitive to sea level change, which tends to favor drier glacial conditions to the west. In Pennsylvanian time, the CPM would have been farther south. Glaciation of the CPM would have amplified the Northern Hemisphere monsoon, even under circular orbit conditions, and driven the ITCZ off the Equator. Precipitation along the coast of equatorial eastern Pangaea would not be limited by moisture availability. The prevailing winds surely would have been laden with moisture evaporated from Paleo-Tethys. Instead, precipitation would have been limited by the location of the convergent flow (and thus the mechanical forcing necessary to drive moist convection). Eastern equatorial Pangaea is particularly sensitive to this effect (Figs. 15f and 16). The model ensemble predicts that precession-driven precipitation variability in the Russian Platform (to the north of the Donets Basin) was in the opposite phase to the Donets Basin (Figs. 15f and 16).

A sufficiently eccentric warm southern summer orbit could melt the CPM and suppress the Northern Hemisphere monsoon, resulting in a much wetter Donets Basin and much drier Russian Platform. Gondwanan ice sheet ablation likely would lag the monsoon changes, so depositional proxies would indicate wetter lowstand conditions. This effect also could explain glacial humidity farther west during Middle Pennsylvanian time

## Tropical Pangaeian Precipitation

N. G. Heavens et al.

Title Page

Abstract

Introduction

Conclusions

References

Tables

Figures



Back

Close

Full Screen / Esc

Printer-friendly Version

Interactive Discussion



(Cecil et al., 2003), when sea level was broadly higher, and thus precipitation was less sensitive to sea level changes. Note, for instance, how far high values of precipitation sensitivity to sea level are displaced from the eastern Pangaeian coastline (Fig. 15b), suggesting that sea level change affects precipitation in more inland areas rather than the coastal areas actually flooded or drained.

In Late Pennsylvanian and Early Permian time, the combined effects of lower greenhouse gases, lower sea level, and potential equatorial mountain glaciation would have favored glacial aridity throughout the tropics. Away from the Equator (particularly ~15° N or S in these simulations), secondary variability in precipitation could be driven by feedback between insolation forcing and the monsoon, resulting in alternating precession pluvials and droughts, particularly when eccentricity was high (Fig. 16). Due to the sea level/precipitation relation, the net amplitude of these pluvials and droughts in the Northern Hemisphere would have been highest when Southern Hemisphere ice sheets were stable or in areas where precipitation sensitivity to sea level was low. Precession pluvials and droughts may be the underlying climatic driver for 5th order cycles, such as those preserved in the North American Midcontinent near the Pennsylvanian-Permian boundary (Olszewski and Patzkowsky, 2003).

None of this complexity is surprising. Different areas of late Cenozoic East Africa have vastly different glacial precipitation regimes (Garcin et al., 2006), a phenomenon which may have been caused by variable responses to precessional forcing and other mechanisms discussed above.

## 5 Summary

Using a fully coupled atmosphere-ocean-land-sea ice model, we have simulated climate during the Asselian and Sakmarian Stages of the Permian to test various mechanisms that could have contributed to glacial-interglacial variability in precipitation over tropical Pangaea. The results of these simulations generally support the idea that equatorial Pangaea, like the Earth generally, was drier at when ice sheets were bigger

## Tropical Pangaeian Precipitation

N. G. Heavens et al.

Title Page

Abstract

Introduction

Conclusions

References

Tables

Figures



Back

Close

Full Screen / Esc

Printer-friendly Version

Interactive Discussion



relative to times when ice sheets were smaller. Glacial aridity in equatorial Pangaea mainly would have been due to sea level fall, which deprived the interior of an important moisture source for precipitation. Other factors capable of contributing to equatorial glacial aridity include potentially lower greenhouse gas levels; and tropical mountain glaciation, if it occurred.

Under low greenhouse gas levels, eccentric orbital conditions, and after a critical point in Pangaeian continental assembly, the precipitation regime in the Pangaeian tropics away from the Equator would have been strongly affected by monsoonal variability forced by the precession cycle. Thus, precession forcing may have been the climatic driver for 5th order cyclicity evident in some sedimentary deposits from Pangaea during this period.

Glaciation of the Central Pangaeian Mountains would have suppressed precipitation in their vicinity, and thus could explain glacial aridity in equatorial Pangaea during Asselian-Sakmarian time. During Middle Pennsylvanian time, the Central Pangaeian Mountains were displaced further southward, and could have amplified (or perhaps initiated) a Northern Hemisphere monsoon over Pangaea. Particular, but plausible relations between orbital forcing, high-latitude glaciation, and tropical mountain glaciation might have resulted in more humid conditions during glacials (lowstands) in exceptional areas of equatorial Pangaea. Precipitation in these areas would need to have been relatively insensitive to changes in sea level, which is plausible if the limiting factor on moist convection in these areas was mechanical forcing rather than moisture availability. The verification and reconstruction of glaciation in the Central Pangaeian Mountains is thus crucial to understanding tropical Pangaeian climate variability during the Late Paleozoic Ice Age.

CPD

8, 1915–1972, 2012

## Tropical Pangaeian Precipitation

N. G. Heavens et al.

Title Page

Abstract

Introduction

Conclusions

References

Tables

Figures

◀

▶

◀

▶

Back

Close

Full Screen / Esc

Printer-friendly Version

Interactive Discussion



## Appendix A

### Paleogeographic base map

The base map for topography/bathymetry uses the Early Permian (280 Ma) reconstruction of Blakey (2008, 2011), hereafter B280, as a template. The base map follows B280 with respect to coastlines and some aspects of bathymetry, such as the placement of trenches along subduction zones (bathymetry of  $-6000$  m). We have not included B280's placement of a hypothetical spreading center in the Panthalassic Ocean (see Ziegler et al., 1997).

Most of the Panthalassic Ocean is given flat bottom bathymetry of  $-4000$  m. The other major ocean basin, the Paleo-Tethys Sea, is given flat bottom bathymetry of  $-3250$  m. B280 suggests Paleo-Tethys was shallower than the Panthalassic, and Celâl Sengör and Atayman (2009) have proposed that the abyssal regions of Paleo-Tethys and the Panthalassic were isolated as early as the Carboniferous. The seaway between Angara and northern Pangaea is given flat bottom bathymetry of  $-2500$  m on its northwestern end, which gradually shallows toward the southeast. This bathymetry is broadly consistent with B280 and the arguments of Gradstein et al. (2004) that this seaway was closed by the beginning of Pennsylvanian time. Furthermore, B280 and Scotese et al. (1997) maps the subduction of the Panthalassic plate underneath this seaway, suggesting the oceanic lithosphere of the seaway is warmer, less dense, and thus thicker (shallower bathymetry) than the Panthalassic plate. A similar rationale justifies  $-2500$  m flat bottom bathymetry for the seaway to the south of Paleo-Tethys.

The mapping of shallower bathymetry near coastlines generally follows B280. The least deep bathymetry likely was ephemerally flooded during glacioeustatic cycles, so it is given a topography of 50 m. B280 maps a shallow interior sea in Gondwanaland between modern South America and Africa. There is evidence for marine faunal exchange between the Parana Basin of Brazil and the Karoo Basin of South Africa in the

CPD

8, 1915–1972, 2012

## Tropical Pangaeian Precipitation

N. G. Heavens et al.

Title Page

Abstract

Introduction

Conclusions

References

Tables

Figures

◀

▶

◀

▶

Back

Close

Full Screen / Esc

Printer-friendly Version

Interactive Discussion



Early Permian that ends by Late Permian time (Ziegler et al., 1997), so the base map follows B280.

The mapping of topography is a compromise between B280 and the ice-free topographic reconstruction during Asselian (292 Ma) time of Rowley (2008), hereafter R292.

Areas mapped in R292 as having topography of 0 m, 200 m, 1000 m are given topography of 100 m, 200 m, and 1500 m respectively. An additional category of 600 m terrain is mapped on the basis of a base map for the Changhsingian created by D. Rowley and used by Kiehl and Shields (2005), hereafter KS251. R292 and B280 disagree somewhat in the placement of high terrain. Mountain ranges in B280 also tend to be wider than R292. The base map generally follows B280 with respect to these matters, though all high terrain can be approximately identified with a topographic feature described by Ziegler et al. (1997). Following Slingerland and Furlong (1989), the core of the Central Pangaeon Mountains (approx. 2000 m contour of R292) are mapped at an altitude of 4000 m, which is comparable to the modern central Andes. Finally, a box average filter was used to smooth the base map at  $3.5^\circ \times 3.5^\circ$  resolution to obtain reasonable slopes.

Figure A1a–c compares three digital elevation models (DEMs): a DEM for the present-day Earth (NOAA NGDC, 2006) deformed to  $0.5^\circ \times 0.5^\circ$ , a resolution identical to the other base maps, and KS251. Figure A1d compares the distributions of topography and bathymetry for the three DEMs. Note that both the base map and KS251 are highly unrealistic, especially in distributing deep bathymetry and high topography. While the present-day DEM used includes topography due to glaciation on Greenland and Antarctica, serious discrepancies between the Modern DEM and the Early Permian DEM would remain even if topography due to land ice were added.

*Acknowledgements.* N. G. Heavens thanks J. T. Kiehl (NCAR) for assistance in designing and implementing the model simulations. This work was supported by the National Science Foundation: EAR-0745961 to N. M. Mahowald; EAR-0746042 to G. S. Soreghan and M. J. Soreghan.

CPD

8, 1915–1972, 2012

## Tropical Pangaeon Precipitation

N. G. Heavens et al.

Title Page

Abstract

Introduction

Conclusions

References

Tables

Figures

◀

▶

◀

▶

Back

Close

Full Screen / Esc

Printer-friendly Version

Interactive Discussion



## References

- Allen, J. P., Fielding, C. R., Gibling, M. R., and Rygel, M. C.: Fluvial response to paleo-equatorial climate fluctuations during the late Paleozoic ice age, *Geol. Soc. Am. Bull.*, 123, 1524–1538, 2011.
- 5 Becq-Giraudon, J.-F., Montenat, C., and Van Den Driessche, J.: Hercynian high-altitude phenomena in the French Massif Central: tectonic implications, *Palaeogeogr. Palaeoclimatol.*, 122, 227–241, 1996.
- Birgenheier, L. P., Fielding, C. R., Rygel, M. C., Frank, T. D., and Roberts, J.: Evidence for Dynamic Climate Change on Sub-10<sup>6</sup>-Year Scales From the Late Paleozoic Glacial Record, Tamworth Belt, New South Wales, Australia, *J. Sediment Res.*, 79, 56–82, doi:10.2110/jsr.2009.013, 2009.
- 10 Blakey, R. C.: Gondwana paleogeography from assembly to breakup – A 500 m.y. odyssey, in: *Resolving the Late Paleozoic Ice Age in Time and Space*, edited by: Fielding, C. R., Frank, T. D., and Isbell, J. L., *Geol. Soc. Am. Spec. Pap.*, 441, 1–28, 2008.
- 15 Blakey, R. C.: Rectangular Global Maps, Northern Arizona University, available at: [http://www2.nau.edu/rcb7/rect\\_globe.html](http://www2.nau.edu/rcb7/rect_globe.html) (last access: 6 March 2012), 2011.
- Bond, W. J., Woodward, F. I., and Midgley, G. F.: The global distribution of ecosystems in a world without fire, *New Phytol.*, 165, 525–538, 2005.
- Boos, W. R. and Kuang, Z.: Dominant control of the South Asian monsoon by orographic insulation versus plateau heating, *Nature*, 463, 218–222, 2010.
- 20 Bordoni, S. and Schneider, T.: 2008, Monsoons as eddy-mediated regime transitions of the tropical overturning circulation, *Nat. Geosci.*, 1, 515–519, 2008.
- Bunker, A. F.: Interaction of the summer monsoon air with the Arabian Sea (preliminary analysis), in: *Proceedings of the Symposium on Meteorological Results of the International Indian Ocean Expedition, Bombay, India, 22–26 July 1965*, Indian Meteorological Department, New Delhi, 3–16, 1965.
- 25 Came, R. E., Eiler, J. M., Veizer, J., Azmy, K., Brand, U., and Weidman, C. R.: Coupling of surface temperatures and atmospheric CO<sub>2</sub> concentrations during the Palaeozoic era, *Nature*, 449, 198–202, 2007.
- 30 Carter, R. M., Abbott, S. T., and Naish, T. R.: Plio-Pleistocene cyclothems from Wanganui Basin, New Zealand: type locality for an astrochronologic time-scale, or template for recognizing ancient glacio-eustasy? *Philos. T. Roy. Soc. A*, 357, 1861–1872, 1999.

## Tropical Pangaeian Precipitation

N. G. Heavens et al.

Title Page

Abstract

Introduction

Conclusions

References

Tables

Figures

◀

▶

◀

▶

Back

Close

Full Screen / Esc

Printer-friendly Version

Interactive Discussion



## Tropical Pangaeon Precipitation

N. G. Heavens et al.

[Title Page](#)[Abstract](#)[Introduction](#)[Conclusions](#)[References](#)[Tables](#)[Figures](#)[◀](#)[▶](#)[◀](#)[▶](#)[Back](#)[Close](#)[Full Screen / Esc](#)[Printer-friendly Version](#)[Interactive Discussion](#)

- Cecil, C. B.: Paleoclimate controls on stratigraphic repetition of chemical and siliciclastic rocks, *Geology*, 18, 533–536, 1990.
- Cecil, C. B., Dulong, F. T., West, R. R., Stamm, R., Wardlaw, B., and Edgar, N. T.: Climate controls on the stratigraphy of a Middle Pennsylvanian cyclothem in North America, in: Climate controls on stratigraphy, edited by: Cecil, C. B. and Edgar, N. T., SEPM Soc. Sedim. Geol. Spec. Publ., 77, 151–182, 2003.
- Celâl Sengör, A. M. and Atayman, S.: The Permian Extinction and the Tethys: An Exercise in Global Geology, *Geol. Soc. Am. Spec. Pap.*, 448, 1–85, 2009.
- Chao, W. C. and Chen, B.: The Origin of Monsoons, *J. Atmos. Sci.*, 58, 3497–3507, 2001.
- Cheng, H., Edwards, R. L., Broecker, W. S., Denton, G. H., Kong, X., Wang, Y., Zhang, R., and Wang, X.: Ice Age Terminations, *Science*, 326, 248–252, 2009.
- Collins, W. D., Bitz, C. M., Blackmon, M. L., Bonan, G. B., Bretherton, C. S., Carton, J. A., Chang, P., Doney, S. C., Hack, J. J., Henderson, T. B., Kiehl, J. T., Large, W. G., McKenna, D. S., Santer, B. D., and Smith, R. D.: The Community Climate System Model Version 3 (CCSM3), *J. Climate*, 19, 2122–2143, 2006.
- Crowley, T. J., Baum, S. K., and Hyde, W. T.: Climate Model Comparison of Laurentide and Gondwanan Glaciations, *J. Geophys. Res.*, 96, 9217–9226, 1991.
- Davydov, V. I., Crowley, J. L., Schmitz, M. D., and Poletaev, V. I.: High-precision U-Pb zircon age calibration of the global Carboniferous time scale and Milankovitch band cyclicity in the Donets Basin, eastern Ukraine, *Geochem. Geophys. Geosy.*, 11, Q0AA04, doi:10.1029/2009GC002736, 2010.
- DiMichele, W. A., Mamay, S. H., Chaney, D. S., Hook, R. W., and Nelson, W. J.: An Early Permian Flora with Late Permian and Mesozoic Affinities from North-Central Texas, *J. Paleontol.*, 75, 449–460, 2001.
- Du Toit, A. L. and Reed, F. R. C.: A Geological Comparison of South America with South Africa, Carnegie Institute of Washington, Washington, DC, 1927.
- Eros, J. M., Montañez, I. P., Osleger, D. A., Davydov, V. I., Nemyrovska, T. I., Poletaev, V. I., and Zhykalyak, M. V.: Sequence stratigraphy and onlap history of the Donets Basin, Ukraine: Insight into Carboniferous icehouse dynamics, *Palaeogeogr. Palaeoclimatol.*, 313–314, 1–25, 2012.
- Fairbanks, R. G.: A 17,000 year glacio-eustatic sea level record: influence of glacial melting rates on the Younger Dryas event and deep ocean circulation, *Nature*, 342, 637–642, 1989.
- Falcon-Lang, H. J. and DiMichele, W. A.: What happened to the Coal Forests during glacial phases?, *Palaios*, 25, 611–617, 2010.

## Tropical Pangaeon Precipitation

N. G. Heavens et al.

Title Page

Abstract

Introduction

Conclusions

References

Tables

Figures

◀

▶

◀

▶

Back

Close

Full Screen / Esc

Printer-friendly Version

Interactive Discussion



- Fielding, C. R., Frank, T. D., and Isbell, J. L.: The late Paleozoic ice age – a review of current understanding and synthesis of global climate patterns, in: *Resolving the Late Paleozoic Ice Age in Time and Space*, edited by: Fielding, C. R., Frank, T. D., and Isbell, J. L., *Geol. Soc. Am. Spec. Pap.*, 441, 343–354, 2008.
- 5 Galtier, J.: A new look at the permineralized flora of Grand-Croix (Late Pennsylvanian, Saint-Etienne basin, France), *Rev. Palaeobot. Palyno.*, 152, 129–140, 2008.
- Garcin, Y., Vincens, A., Williamson, D., Guiot, J., and Buchet, G.: Wet phases in tropical southern Africa during the last glacial period, *Geophys. Res. Lett.*, 33, L07703, doi:10.1029/2005GL025531, 2006.
- 10 Gerasimov, I. P. and Markov, K. K.: *The Glacial Period on the USSR Territory*, USSR Academy of Sciences Publishers, Moscow, 1939.
- Gibbs, M. T., Rees, P. M., Kutzbach, J. E., Ziegler, A. M., Behling, P. J., and Rowley, D. B.: Simulations of Permian Climate and Comparisons with Climate-Sensitive Sediments, *J. Geology*, 110, 33–55, 2002.
- 15 Gough, D. O.: Solar interior structure and luminosity variations, *Sol. Phys.*, 74, 21–34, 1981.
- Gradstein, F. M., Ogg, J. G., Smith, A. G.: *A Geologic Time Scale 2004*, Cambridge University Press, Cambridge, UK, 2004.
- Held, I. M. and Soden, B. J.: Robust responses of the hydrological cycle to global warming, *J. Climate*, 19, 3354–3360, 2006.
- 20 Horton, D. E. and Poulsen, C. J.: Paradox of late Paleozoic glacioeustasy, *Geology*, 37, 715–718, 2009.
- Horton, D. E., Poulsen, C. J., and Pollard, D.: Orbital and CO<sub>2</sub> forcing of late Paleozoic continental ice sheets, *Geophys. Res. Lett.*, 34, L19708, 2007.
- Horton, D. E., Poulsen, C. J., and Pollard, D.: Influence of high-latitude vegetation feedbacks on late Palaeozoic glacial cycles, *Nat. Geosci.*, 3, 572–577, 2010.
- 25 Hoyt, D. V.: Percent of Possible Sunshine and the Total Cloud Cover, *Mon. Weather Rev.*, 105, 648–652, 1977.
- IPCC: *Climate change 2001: The scientific basis. Contribution of Working Group I to the Third Assessment Report of the Intergovernmental Panel on Climate*, edited by: Houghton, J. T., Ding, Y., Griggs, D. J., Noguera, M., Van der Linden, P. J., Dai, X., Maskell, K., and Johnson, C. A., Cambridge University Press, Cambridge and New York, 2001.
- 30

**Tropical Pangaeian  
Precipitation**

N. G. Heavens et al.

[Title Page](#)[Abstract](#)[Introduction](#)[Conclusions](#)[References](#)[Tables](#)[Figures](#)[◀](#)[▶](#)[◀](#)[▶](#)[Back](#)[Close](#)[Full Screen / Esc](#)[Printer-friendly Version](#)[Interactive Discussion](#)

- Isbell, J. L., Lenaker, P. A., Askin, R. A., Miller, M. F., and Babcock, L. E.: Reevaluation of the timing and extent of late Paleozoic glaciation in Gondwana: Role of the Transantarctic Mountains, *Geology*, 31, 977–980, 2003a.
- Isbell, J. L., Miller, M. F., Wolfe, K. L., and Lenaker, P. A.: Timing of late Paleozoic glaciation in Gondwana: Was glaciation responsible for the development of northern hemisphere cyclotheams?, in: *Extreme depositional environments: Mega end members in geologic time*, edited by: Chan, M. A. and Archer, A. W., *Geol. Soc. Am. Spec. Pap.*, 370, 5–24, 2003b.
- Joseph, P. V. and Sijikumar, S.: Intraseasonal Variability of the Low-Level Jet Stream of the Asian Summer Monsoon, *J. Atmos. Sci.*, 17, 1449–1458, 2004.
- Kaplan, J. O., Bigelow, N. H., Prentice, I. C., Harrison, S. P., Bartlein, P. J., Christensen, T. R., Cramer, W., Matveyeva, N. V., McGuire, A. D., Murray, D. F., Razzhivin, V. Y., Smith, B., Walker, D. A., Anderson, P. M., Andreev, A. A., Brubaker, L. B., Edwards, M. E., and Lozhkin, A. V.: Climate change and Arctic ecosystems: 2. Modeling, paleodata-model comparisons, and future projections, *J. Geophys. Res.*, 108, 8171, doi:10.1029/2002JD002559, 2003.
- Kiehl, J. T. and Shields, C. A.: Climate simulation of the latest Permian: Implications for mass extinction, *Geology*, 33, 757–760, 2005.
- Kiehl, J. T., Shields, C. A., Hack, J. J., and Collins, W. D.: The Climate Sensitivity of the Community Climate System Model Version 3 (CCSM3), *J. Climate*, 19, 2584–2596, 2006.
- Köppen, W. and Wegener, A.: *Die Klimate die geologischen Vorzeit*, Gebrüder Borntraeger, Berlin, Germany, 1924.
- Kutzbach, J. E. and Gallimore, R. G.: Pangaeian Climates: Megamonsoons of the Megacontinent, *J. Geophys. Res.*, 94, 3341–3357, 1989.
- Kutzbach, J. E. and Ziegler, A. M.: Simulation of Late Permian Climate and Biomes with an Atmosphere-Ocean Model: Comparisons with Observations, *Philos. T. Roy. Soc. B*, 341, 327–340, 1993.
- Kutzbach, J. E., Liu, X., Liu, Z., and Chen, G.: Simulation of the evolutionary response of global summer monsoons to orbital forcing over the past 280,000 years, *Clim. Dynam.*, 30, 567–579, 2008.
- Laskar, J., Robutel, P., Joutel, F., Gastineau, M., Correia, A. C. M., and Levrard, B.: A long term numerical solution for the insolation quantities of the Earth, *Astron. Astrophys.*, 428, 261–285, 2004.
- Liu, H., Aris-Brosou, S., Probert, I., and de Vargas, C.: A Timeline of the Environmental Genetics of the Haptophytes, *Mol. Biol. Evol.*, 27, 161–176, 2010.

## Tropical Pangaeian Precipitation

N. G. Heavens et al.

[Title Page](#)[Abstract](#)[Introduction](#)[Conclusions](#)[References](#)[Tables](#)[Figures](#)[◀](#)[▶](#)[◀](#)[▶](#)[Back](#)[Close](#)[Full Screen / Esc](#)[Printer-friendly Version](#)[Interactive Discussion](#)

- Lythe, M. B., Vaughan, D. G., and the BEDMAP Consortium: BEDMAP: A new ice thickness and subglacial topographic model, *J. Geophys. Res.*, 106, 11335–11351, 2001.
- Mahowald, N. M.: Anthropocene changes in desert area: Sensitivity to climate model predictions, *Geophys. Res. Lett.*, 34, L18817, doi:10.1029/2007GL030472, 2007.
- 5 Mahowald, N. M., Ward, D. S., Kloster, S., Flanner, M. G., Heald, C. L., Heavens, N. G., Hess, P. G., and Lamarque, J.-F.: Aerosol impacts on climate and biogeochemistry, *Annu. Rev. Env. Resour.*, 36, 45–74, 2011.
- Meehl, G. A. and Arblaster, J. M.: Mechanisms for projected future changes in south Asian monsoon precipitation, *Clim. Dynam.*, 21, 659–675, 2003.
- 10 Melvin, J., Sprague, R. A., and Heine, C. J.: From bergs to ergs: The Late Paleozoic Gondwanan glaciation and its aftermath in Saudi Arabia, in: Late Paleozoic glacial events and postglacial transgressions in Gondwana, edited by: López-Gamundí, O. R. and Buatois, L. A., *Geol. Soc. Am. Spec. Pap.*, 468, 37–80, 2010.
- Montañez, I. P., Tabor, N. J., Niemeier, D., DiMichele, W. A., Frank, T. D., Fielding, C. R., Isbell, J. L., Birgenheier, L. P., and Rygel, M. C.: CO<sub>2</sub>-Forced Climate and Vegetation Instability During Late Paleozoic Glaciation, *Science*, 315, 87–91, 2007.
- NOAA NGDC: 2-Minute Gridded Global Relief Data (ETOPO2v2) June, 2006, available at: <http://www.ngdc.noaa.gov/mgg/fliers/01mgg04.html> (last access: 6 March 2012), 2006.
- Olson, E. C.: Community Evolution and the Origin of Mammals, *Ecology*, 47, 291–302, 1966.
- 20 Olszewski, T. D. and Patzkowsky, M. E.: From Cyclothems to Sequences: The Record of Eustasy and Climate on an Icehouse Epeiric Platform (Pennsylvanian-Permian, North American Midcontinent), *J. Sediment Res.*, 73, 15–30, 2003.
- Otto-Bliesner, B.: The Role of Mountains, Polar Ice, and Vegetation in Determining the Tropical Climate During the Middle Pennsylvanian: Climate Model Simulations, in: Climate controls on stratigraphy, edited by: Cecil, C. B. and Edgar, N. T., *SEPM Soc. Sedim. Geol. Spec. Publ.*, 77, 227–238, 2003.
- 25 Otto-Bliesner, B. L., Brady, E. C., Clauzet, G., Tomas, R., Levis, S., and Kothavala, Z.: Last Glacial Maximum and Holocene Climate in CCSM3, *J. Climate*, 19, 2526–2544, 2006.
- Peltier, W. R.: Global glacial isostasy and the surface of the ice-age Earth: the ICE-5G (VM2) model and GRACE, *Annu. Rev. Earth Pl. Sc.*, 32, 111–149, 2004.
- 30 Perlmutter, M. A. and Matthews, M. D.: Global cyclostratigraphy – a model, in: Quantitative Dynamic Stratigraphy, edited by: Cross, T. A., Prentice Hall, Englewood Cliffs, New Jersey, 223–260, 1989.

## Tropical Pangaeen Precipitation

N. G. Heavens et al.

[Title Page](#)[Abstract](#)[Introduction](#)[Conclusions](#)[References](#)[Tables](#)[Figures](#)[◀](#)[▶](#)[◀](#)[▶](#)[Back](#)[Close](#)[Full Screen / Esc](#)[Printer-friendly Version](#)[Interactive Discussion](#)

- Petit, J. R., Mournier, L., Jouzel, J., Korotkevich, Y. S., Kotlyakov, V. I., and Lorius, C.: Palaeoclimatological and chronological implications of the Vostok core dust record, *Nature*, 343, 56–58, 1990.
- Petit, J. R., Jouzel, J., Raynaud, D., Barkov, N. I., Barnola, J.-M., Basile, I., Bender, M., Chappellaz, J., Davis, M., Delaygue, G., Delmotte, M., Kotlyakov, V. M., Legrand, M., Lipenkov, V. Y., Lorius, C., Pépin, L., Ritz, C., Saltzman, E., and Stievenard, M.: Climate and atmospheric history of the past 420,000 years from the Vostok ice core, Antarctica, *Nature*, 399, 429–436, 1999.
- Peyser, C. E. and Poulsen, C. J.: Controls on Permo-Carboniferous precipitation over tropical Pangaea: A GCM sensitivity study, *Palaeogeogr. Palaeocl.*, 268, 181–192, 2008.
- Pough, F. H., Janis, C. M., and Heiser, J. B.: *Vertebrate Life*, Benjamin Cummings, San Francisco, CA, 2008.
- Poulsen, C. J., Pollard, D., Montañez, I. P., and Rowley, D.: Late Paleozoic tropical climate response to Gondwanan deglaciation, *Geology*, 35, 771–774, 2007.
- Rea, D. K.: The Paleoclimatic Record Provided by Eolian Deposition in the Deep Sea, *Rev. Geophys.*, 32, 159–195, 1994.
- Rosenbloom, N., Shields, C., Brady, E., Levis, S., Yeager, S., Using CCSM3 for Paleoclimate Applications, NCAR Technical Note 483, Boulder, CO, 2011.
- Rowley, D.: 2003 Revised Permian Paleogeographic Maps, available at: [http://geosci.uchicago.edu/~rowley/Rowley/Revised\\_Permian\\_Maps.html](http://geosci.uchicago.edu/~rowley/Rowley/Revised_Permian_Maps.html) (last access: 6 March 2012), 2008.
- Schwarzacher, W.: Milankovitch type cycles in the Lower Carboniferous of NW Ireland, *Terra Nova*, 1, 468–473, 1989.
- Scotese, C. R.: *Paleogeographic Atlas*, PALEOMAP Progress Report, 90-0497, Department of Geology, University of Texas at Arlington, Arlington, Texas, 1997.
- Shi, G. R. and Waterhouse, J. B.: Late Paleozoic global changes affecting high-latitude environments and biotas: An introduction, *Palaeogeogr. Palaeocl.*, 298, 1–16, 2010.
- Slingerland, R. and Furlong, K. P.: Geodynamic and geomorphic evolution of the Permo-Triassic Appalachian mountains, *Geomorphology*, 2, 23–37, 1989.
- Soreghan, G. S.: The impact of glacioclimatic change on Pennsylvanian cyclostratigraphy, in: *Pangea–Global environments and resources*, edited by: Embry, A. F., Beauchamp, B., and Glass, D. J., *Can. Soc. Petrol. Geol. Mem.*, 17, 523–543, 1994.
- Soreghan, G. S.: Walther’s Law, climate change, and upper Paleozoic cyclostratigraphy in the Ancestral Rocky Mountains, *J. Sediment Res.*, 67, 1001–1004, 1997.

## Tropical Pangaeen Precipitation

N. G. Heavens et al.

[Title Page](#)[Abstract](#)[Introduction](#)[Conclusions](#)[References](#)[Tables](#)[Figures](#)[Back](#)[Close](#)[Full Screen / Esc](#)[Printer-friendly Version](#)[Interactive Discussion](#)

- Soreghan, G. S., Soreghan, M. J., and Hamilton, M. A.: Origin and paleoclimatic significance of tropical silt in the Late Paleozoic icehouse, *Palaeogeogr. Palaeoclimatol.*, 268, 234–259, 2008a.
- Soreghan, G. S., Soreghan, M. J., Poulsen, C. J., Young, R. A., Eble, C. F., Sweet, D. E., and Davogustto, O. C.: Anomalous cold in the Pangaeen tropics, *Geology*, 36, 659–662, 2008b.
- 5 Soreghan, G. S., Soreghan, M. J., Sweet, D. E., and Moore, K. D.: Hot Fan or Cold Outwash?: Hypothesized Proglacial Deposition in the Upper Paleozoic Cutler Formation, Western Tropical Pangaea, *J. Sediment Res.*, 79, 495–522, 2009.
- Stanley, S. M.: *Earth System History*, W. H. Freeman and Co., New York, NY, 1999.
- Sues, H.-D. and Reisz, R. R.: Origins and early evolution of herbivory in tetrapods, *Trends Ecol. Evol.*, 13, 141–145, 1998.
- 10 Sweet, D. E. and Soreghan, G. S.: Polygonal cracking in coarse clastics records cold temperatures in the equatorial Fountain Formation (Pennsylvanian-Permian, Colorado), *Palaeogeogr. Palaeoclimatol.*, 268, 193–204, 2008.
- Tabor, N. J. and Poulsen, C. J.: Palaeoclimate across the Late Pennsylvanian-Early Permian tropical palaeolatitudes: A review of climate indicators, their distribution, and relation to palaeophysiographic climate factors, *Palaeogeogr. Palaeoclimatol.*, 268, 293–310, 2008.
- 15 Veevers, J. J. and Powell, C. M.: Late Paleozoic glacial episodes in Gondwanaland reflected in transgressive-regressive depositional sequences in Euramerica, *Geol. Soc. Am. Bull.*, 98, 475–487, 1987.
- 20 Wang, B., Wu, R., and Lau, K.-M.: Interannual Variability of the Asian Summer Monsoon: Contrasts between the Indian and the Western North Pacific-East Asian Monsoons, *J. Climate*, 14, 4073–4090, 2001.
- Wanless, H. R. and Shepard, F. P.: Sea level and climatic change related to Late Paleozoic cycles, *Geol. Soc. Am. Bull.*, 47, 1177–1206, 1936.
- 25 Webster, P. J. and Fasullo, J.: Monsoon: Dynamical Theory, in: *Encyclopedia of Atmospheric Sciences*, edited by: Holton, J. R., Curry, J. A., and Pyle, J. A., Academic Press, San Diego, CA, 1370–1385, 2003.
- Williams Jr., R. S. and Ferrigno, J. G.: Satellite image atlas of glaciers of the world: United State Geological Survey Fact Sheet 2005–3056, available at: <http://pubs.usgs.gov/fs/2005/3056> (last access: 23 May 2012), 2005.
- 30 Wilson, J. P. and Knoll, A. H.: A physiologically explicit morphospace for tracheid-based water transport in modern and extinct seed plants, *Paleobiology*, 36, 335–355, 2010.

## Tropical Pangaeon Precipitation

N. G. Heavens et al.

Title Page

Abstract

Introduction

Conclusions

References

Tables

Figures

◀

▶

◀

▶

Back

Close

Full Screen / Esc

Printer-friendly Version

Interactive Discussion



- Witzke, B. J.: Palaeoclimatic constraints for Palaeozoic Palaeolatitudes of Laurentia and Euramerica, in: Palaeozoic Palaeogeography and Biogeography, edited by: McKerrow, W. S. and Scotese, C. R., Geol. Soc. Am. Mem., 12, 57–73, 1990.
- 5 Yeager, S. G., Shields, C. A., Large, W. G., and Hack, J. J.: The Low-Resolution CCSM3, J. Climate, 19, 2545–2566, 2006.
- Ziegler, A. M., Hulver, M. L., and Rowley, D. B.: Permian World Topography and Climate, in: Late Glacial and Postglacial Environmental Changes: Quaternary, Carboniferous-Permian, and Proterozoic, edited by: Martini, I. P., Oxford University Press, Oxford, UK, 111–146, 1997.
- 10 Zug, G. R., Vitt, L. J., and Caldwell, J. P.: Herpetology: An Introductory of Biology of Amphibians and Reptiles, Academic Press, San Diego, CA, 2001.

## Tropical Pangaeian Precipitation

N. G. Heavens et al.

Title Page

Abstract

Introduction

Conclusions

References

Tables

Figures

◀

▶

◀

▶

Back

Close

Full Screen / Esc

Printer-friendly Version

Interactive Discussion



**Table 1.** Greenhouse gas scenarios.

Scenario	$p\text{CO}_2$ (ppmv)	$p\text{CH}_4$ (ppbv)	$p\text{N}_2\text{O}$ (ppbv)
GG2500	2500	5570	311
GG250	250	530	311

## Tropical Pangaeon Precipitation

N. G. Heavens et al.

Title Page

Abstract

Introduction

Conclusions

References

Tables

Figures

◀

▶

◀

▶

Back

Close

Full Screen / Esc

Printer-friendly Version

Interactive Discussion



**Table 2.** Glaciation configurations.

Name	Area ( $10^6 \text{ km}^2$ )	Volume ( $10^6 \text{ km}^3$ )	Sea Level Equivalent (m) <sup>a</sup>
ICES	11	21	65
ICEB	17	44	107
ICEH	79	44 <sup>c</sup>	107 <sup>c</sup>
Present <sup>b</sup>	16	33	80

<sup>a</sup> Without isostatic adjustment. <sup>b</sup> Williams and Ferrigno (2005).

<sup>c</sup> While ICEH has no additional glacial topography relative to ICEB, keep in mind that the ice volume and equivalent sea level change of land ice covering the same area as ICEH is likely much greater than shown here.

Tropical Pangaeon  
Precipitation

N. G. Heavens et al.

**Table 3.** Simulations of Late Paleozoic Climate.

Case Number <sup>a</sup>	Name	Greenhouse gas scenario	Sea Level	Vegetation scenario	Glacial configuration	Obliquity (°)	Eccentricity	Longitude of Perihelion (°) <sup>b</sup>
1	greenhouse.base	GG2500	SL100	Uniform	None	23.5	0	0
2	icehouse.base	GG250	SL0	Uniform	None	23.5	0	0
3	greenhouse.noglaciati	GG2500	SL100	V2500	None	23.5	0	0
4	gh.ng.ecc	GG2500	SL100	V2500	None	22.0	0.057	270
5	gh.ng.ecc4	GG2500	SL100	V2500	None	25.0	0.057	90
6	greenhouse.glaciati	GG2500	SL100	V2500	ICES	23.5	0	0
7	icehouse.highseale	GG250	SL100	V250	None	23.5	0	0
8	icehouse.noglaciati	GG250	SL0	V250	None	23.5	0	0
9	ih.ng.ecc	GG250	SL0	V250	None	22.0	0.057	270
10	ih.ng.ecc4	GG250	SL0	V250	None	25.0	0.057	90
11	icehouse.glaciati	GG250	SL0	V250	ICES	23.5	0	0
12	icehouse.glaciati	GG250	SL0	V250	ICEB	23.5	0	0
13	ih.g.b.ecc	GG250	SL0	V250	ICEB	22.0	0.057	270
14	ih.g.b.ecc2	GG250	SL0	V250	ICEB	22.0	0.057	90
15	ih.g.b.ecc3	GG250	SL0	V250	ICEB	25.0	0.057	270
16	ih.g.b.ecc4	GG250	SL0	V250	ICEB	25.0	0.057	90
17	icehouse.glaciati	GG250	SL0	V250	ICEH	23.5	0	0
18	ih.g.h.ecc	GG250	SL0	V250	ICEH	22.0	0.057	270
19	ih.g.h.ecc4	GG250	SL0	V250	ICEH	25.0	0.057	90

<sup>a</sup> Identical case numbering is used in Table 4, Fig. 2, and is referred to in the text. <sup>b</sup> Following the convention that the longitude of perihelion is 0° at northern vernal equinox.

Title Page

Abstract

Introduction

Conclusions

References

Tables

Figures

◀

▶

◀

▶

Back

Close

Full Screen / Esc

Printer-friendly Version

Interactive Discussion



## Tropical Pangaeon Precipitation

N. G. Heavens et al.

**Table 4.** Annual mean results.

Case Number*	Name	Sfc. $T$ (°C)	Land	Ocean	Tropical	Precip. (mm)	Land	Ocean	Tropical	Sea Ice (% Ocean)
1	greenhouse.base	24.1	21.9	24.8	31.2	1210	920	1310	1490	0.02
2	icehouse.base	16.1	12.3	17.5	24.7	1000	600	1110	1280	2.2
3	greenhouse.vegetation	23.4	21.4	24.2	30.9	1190	840	1310	1480	0.05
4	gh.ng.ecc	23.4	21.3	24.1	31.2	1190	850	1310	1470	0.08
5	gh.ng.ecc4	23.6	21.5	24.3	30.8	1200	860	1310	1490	0.02
6	greenhouse.glaciation.small	22.7	18.9	24.0	31.1	1170	770	1310	1470	0.21
7	icehouse.highsealevel	13.4	7.7	15.4	23.3	980	590	1110	1300	4.8
8	icehouse.noglaciation	14.5	10.1	16.1	24.2	960	520	1110	1260	4.1
9	ih.ng.ecc	14.4	9.8	15.9	24.3	960	530	1110	1260	4.0
10	ih.ng.ecc4	14.7	10.5	16.2	23.9	960	540	1110	1270	4.1
11	icehouse.glaciation.small	13.1	6.7	15.3	24.0	940	480	1090	1240	5.8
12	icehouse.glaciation.big	13.0	4.9	15.9	24.2	940	490	1100	1260	4.4
13	ih.g.b.ecc	12.9	4.9	15.7	24.4	950	490	1100	1260	5.3
14	ih.g.b.ecc2	12.6	4.7	15.4	24.3	940	490	1100	1260	6.4
15	ih.g.b.ecc3	13.1	5.1	15.9	24.0	940	500	1100	1250	4.6
16	ih.g.b.ecc4	13.1	5.1	15.9	24.0	950	500	1100	1260	4.5
17	icehouse.glaciation.huge	1.8	-8.4	5.3	18.4	750	250	920	1090	24.4
18	ih.g.h.ecc	0.5	-9.2	3.9	18.0	730	260	890	1080	27.1
19	ih.g.h.ecc4	3.1	-7.6	6.8	18.8	770	270	940	1110	21.6
20	pic1	13.8	8.4	16.1	25.4	990	760	1090	1330	6.8
21	pic2	13.4	7.5	15.8	25.3	980	740	1090	1320	7.1

\* Identical case numbering is used in Table 3, Fig. 2, and is referred to in the text.

Title Page

Abstract

Introduction

Conclusions

References

Tables

Figures

◀

▶

◀

▶

Back

Close

Full Screen / Esc

Printer-friendly Version

Interactive Discussion



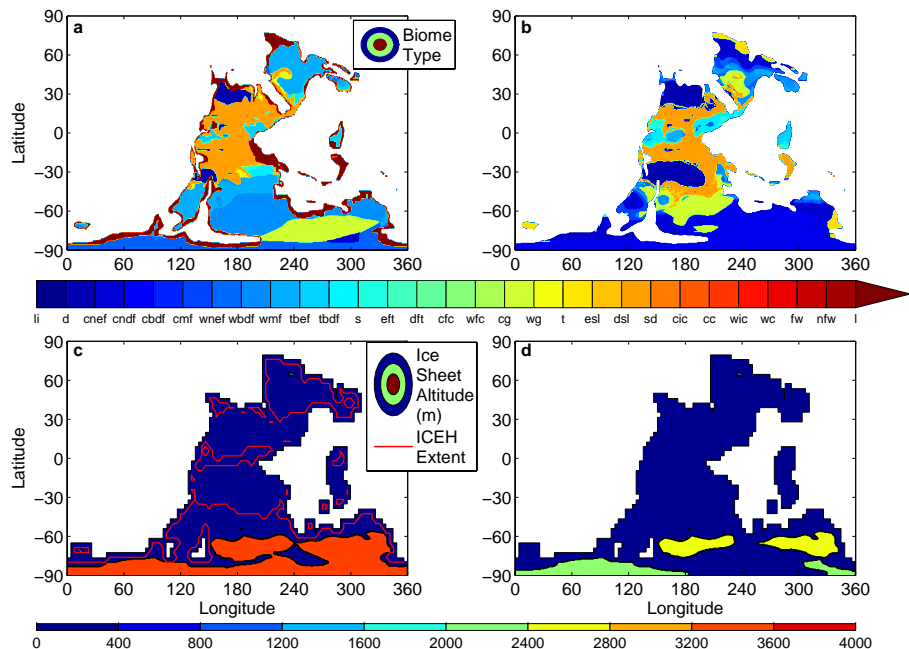


**Fig. 1.** Prescribed vegetation, sea level, and glaciation scenarios: **(a)** V2500 with lake biomes from SL100 imposed; **(b)** V250; **(c)** ICEB and ICEH; **(d)** ICES. Blank space in biome maps is ocean. Abbreviations for biome types in key below Fig. 1a and b: li: land ice; d: desert; cnef: cool needleleaf evergreen forest; cndf: cool needleleaf deciduous forest; cbdf: cool broadleaf deciduous forest; cmf: cool mixed forest; wnef: warm needleleaf evergreen forest; wbdf: warm broadleaf deciduous forest; wmf: warm mixed forest; tbe: tropical broadleaf evergreen forest; tbd: tropical broadleaf deciduous forest; s: savanna; eft: evergreen forest tundra; dft: deciduous forest tundra; cfc: cool forest crop; wfc: warm forest crop; cg: cool grassland; wg: warm grassland; t: tundra; esl: evergreen shrub land; dsl: deciduous shrub land; sd: semi-desert; cic: cool irrigated crop; cc: cool crop; wic: warm irrigated crop; wc: warm crop; fw: forest wetland; nfw: non-forest wetland; l: lake.

**Tropical Pangaeon  
Precipitation**

N. G. Heavens et al.

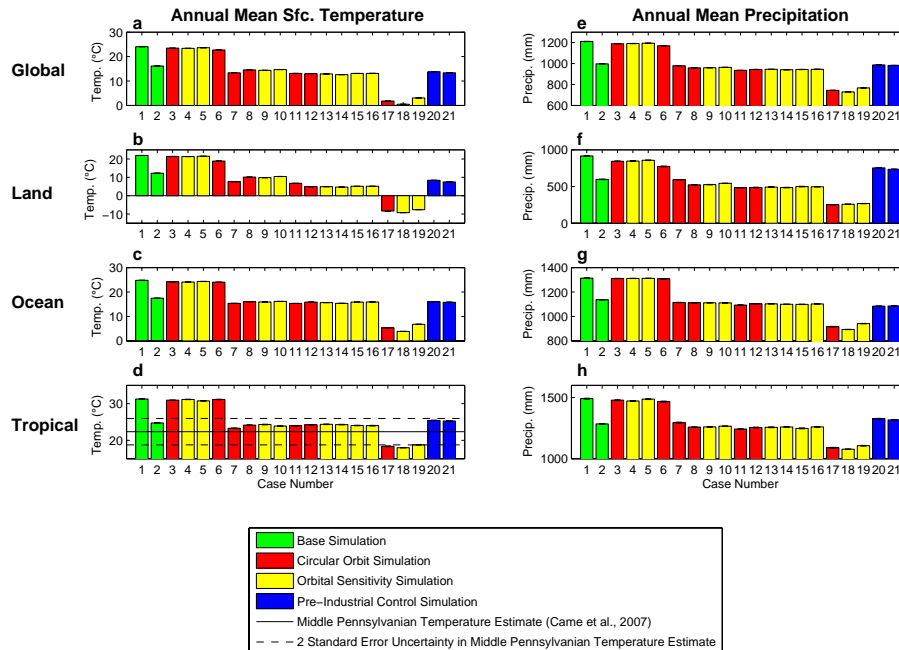


**Fig. 2.** Mean temperature and precipitation analysis of the late Paleozoic climate simulations, as labeled. Error bars mark the  $2\sigma$  confidence interval of the mean ( $\sigma$  = the standard error of the mean). Case numbering matches that of Tables 3 and 4 and the in-text references.

Title Page

Abstract Introduction

Conclusions References

Tables Figures

◀ ▶

◀ ▶

Back Close

Full Screen / Esc

Printer-friendly Version

Interactive Discussion



**Tropical Pangaeon  
Precipitation**

N. G. Heavens et al.

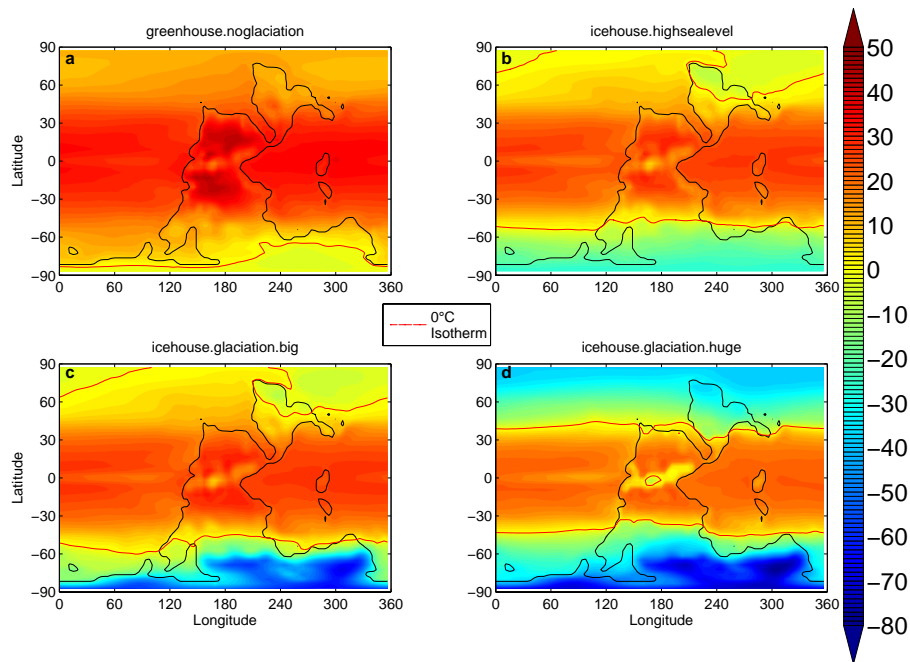


**Fig. 3.** Annual mean temperature (°C) for the labeled simulations.

Title Page

Abstract

Introduction

Conclusions

References

Tables

Figures

◀

▶

◀

▶

Back

Close

Full Screen / Esc

Printer-friendly Version

Interactive Discussion



**Tropical Pangaeian  
Precipitation**

N. G. Heavens et al.

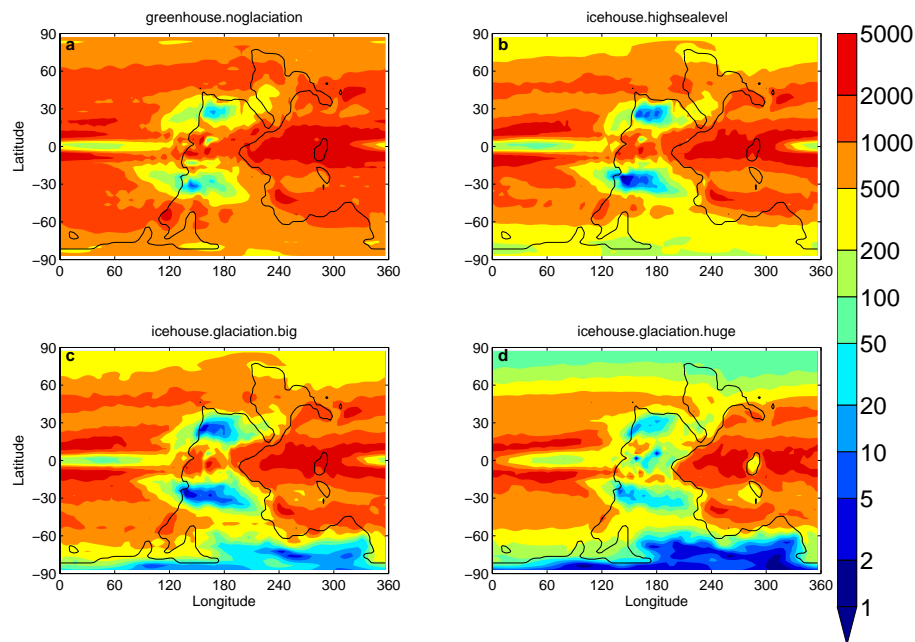


**Fig. 4.** Annual mean precipitation (mm) for the labeled simulations.

[Title Page](#)[Abstract](#)[Introduction](#)[Conclusions](#)[References](#)[Tables](#)[Figures](#)[◀](#)[▶](#)[◀](#)[▶](#)[Back](#)[Close](#)[Full Screen / Esc](#)[Printer-friendly Version](#)[Interactive Discussion](#)

## Tropical Pangaeon Precipitation

N. G. Heavens et al.

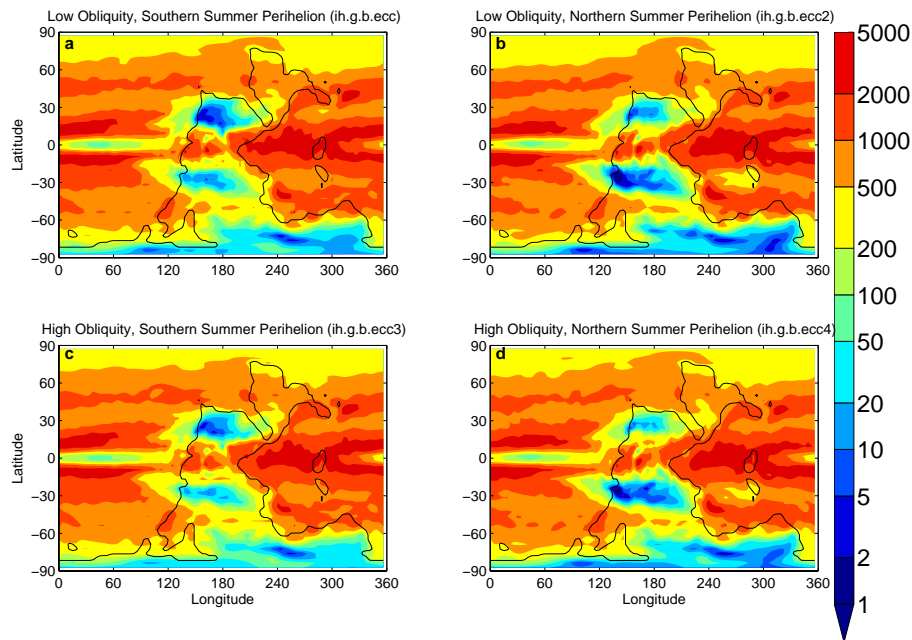


**Fig. 5.** Annual mean precipitation (mm) for the labeled simulations.

[Title Page](#)[Abstract](#)[Introduction](#)[Conclusions](#)[References](#)[Tables](#)[Figures](#)[◀](#)[▶](#)[◀](#)[▶](#)[Back](#)[Close](#)[Full Screen / Esc](#)[Printer-friendly Version](#)[Interactive Discussion](#)

## Tropical Pangaeon Precipitation

N. G. Heavens et al.

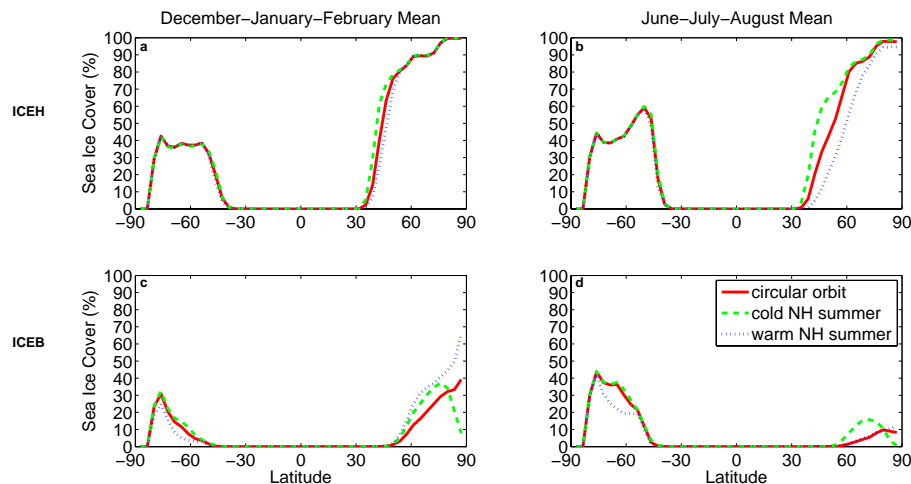


**Fig. 6.** Mean seasonal sea ice cover (% of all area at a given latitude covered by sea ice) for simulations using the glacial configurations labeled: **(a and b)**: “circular orbit” refers to icehouse.glaciation.huge, “cold NH summer” refers to ih.g.h.ecc, and “warm NH summer” refers to ih.g.h.ecc4; **(c and d)**: “circular orbit” refers to icehouse.glaciation.big, “cold NH summer” refers to ih.g.b.ecc, and “warm NH summer” refers to ih,g.b.ecc4.

Title Page

Abstract

Introduction

Conclusions

References

Tables

Figures

◀

▶

◀

▶

Back

Close

Full Screen / Esc

Printer-friendly Version

Interactive Discussion



Tropical Pangaeian  
Precipitation

N. G. Heavens et al.

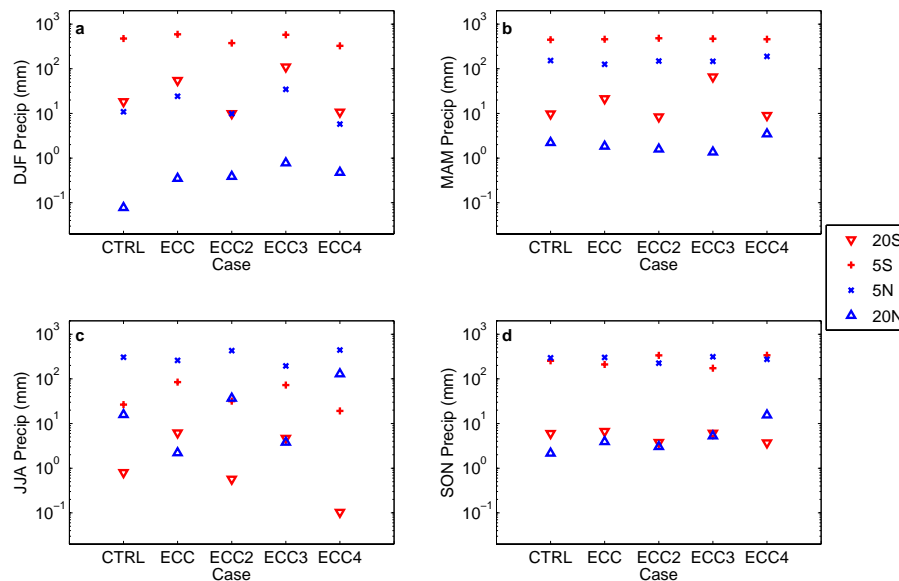


**Fig. 7.** Comparison of the seasonal variability of Pangaeian sector (146.25°–191.25° longitude) non-water area (sum of ocean and lake fraction is equal to 0%) precipitation in the icehouse simulation that uses the big polar ice configuration (icehouse.glaciation.big) and its associated orbital parameter sensitivity experiments (ih.g.b.eccx).

Title Page

Abstract

Introduction

Conclusions

References

Tables

Figures

◀

▶

◀

▶

Back

Close

Full Screen / Esc

Printer-friendly Version

Interactive Discussion



Tropical Pangaeian  
Precipitation

N. G. Heavens et al.

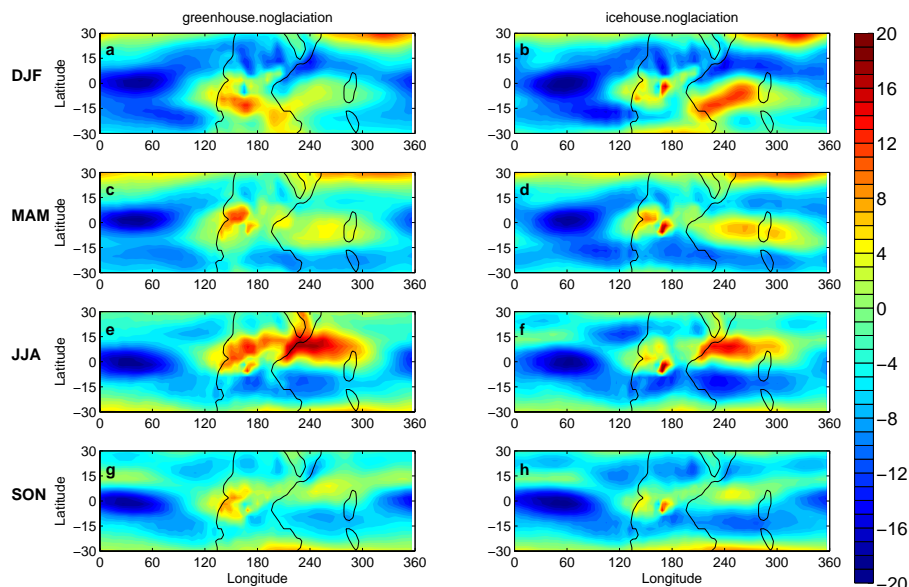


**Fig. 8.** Seasonal variability in mean zonal winds at 850hPa ( $\text{m s}^{-1}$ ) in two simulations with strong (greenhouse.noglaciation) and weak (icehouse.noglaciation) Pangaeian megamonsoons, as labeled.

Title Page

Abstract

Introduction

Conclusions

References

Tables

Figures

◀

▶

◀

▶

Back

Close

Full Screen / Esc

Printer-friendly Version

Interactive Discussion



Tropical Pangaeian  
Precipitation

N. G. Heavens et al.

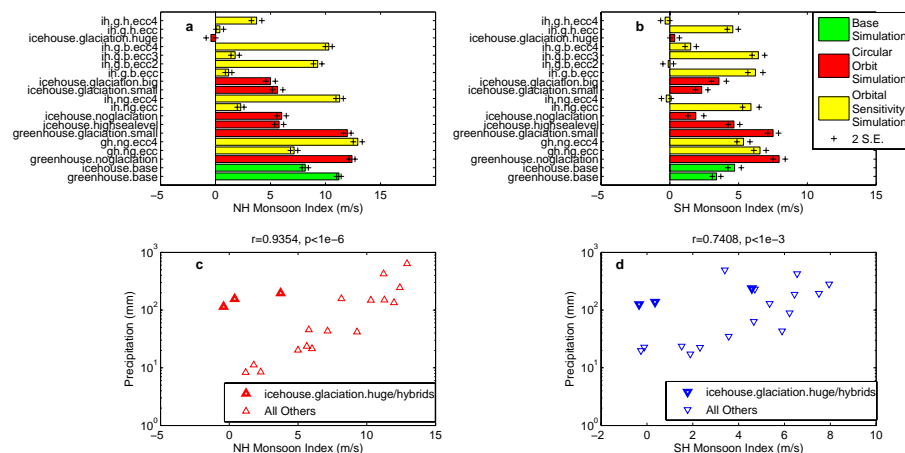


**Fig. 9.** (a) Inter-simulation comparison of Northern Hemisphere monsoon index: difference between mean JJA Pangaeian sector ( $146.25^{\circ}$ – $191.25^{\circ}$  longitude) 850 hPa zonal winds at  $9^{\circ}$  N and  $24^{\circ}$  N; (b) as in (a), but for the Southern Hemisphere; (c) Northern Hemisphere monsoon index vs. zonal average mean annual precipitation over non-water areas of the Pangaeian sector at  $20^{\circ}$  N, linear correlation coefficient (excluding icehouse.glaciation.huge and its hybrid simulations) and p-value between monsoon index and  $\log_{10}$  precipitation are displayed at the top of the panel; (d) as in (c), but for the Southern Hemisphere.

Title Page

Abstract

Introduction

Conclusions

References

Tables

Figures

◀

▶

◀

▶

Back

Close

Full Screen / Esc

Printer-friendly Version

Interactive Discussion



Tropical Pangaeian  
Precipitation

N. G. Heavens et al.

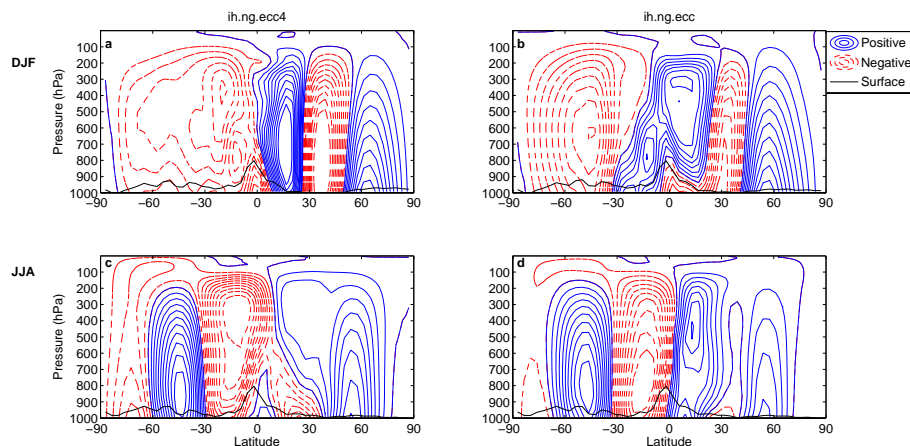


**Fig. 10.** Seasonal mean zonal average meridional streamfunction in the Pangaeian sector ( $146.25^{\circ}$ – $191.25^{\circ}$  longitude). Contour frequency is  $5 \times 10^{10} \text{ kg s}^{-1}$ . The plotting convention follows the left-hand rule; positive streamfunction therefore indicates clockwise meridional flow.

Title Page

Abstract

Introduction

Conclusions

References

Tables

Figures

◀

▶

◀

▶

Back

Close

Full Screen / Esc

Printer-friendly Version

Interactive Discussion



Tropical Pangaeon  
Precipitation

N. G. Heavens et al.

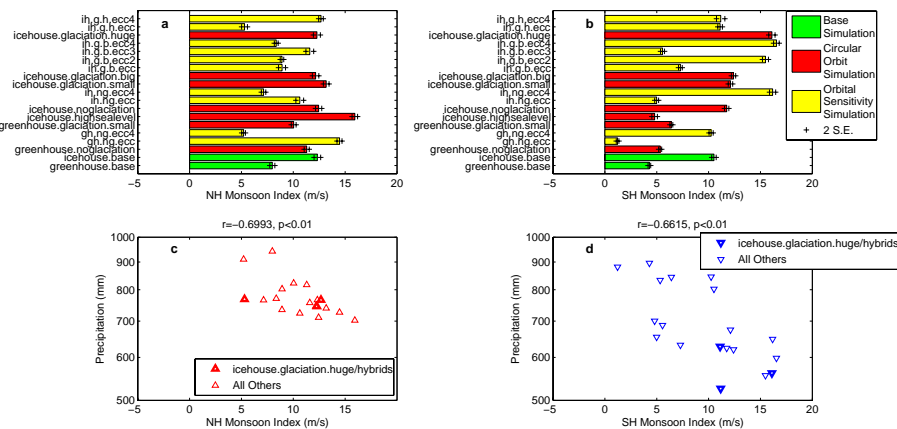


**Fig. 11.** Same as Fig. 9, except indices and averages are over the domain of the Paleo-Tethyan sector ( $232.5^{\circ}$ – $281.5^{\circ}$  longitude).

Title Page

Abstract

Introduction

Conclusions

References

Tables

Figures

◀

▶

◀

▶

Back

Close

Full Screen / Esc

Printer-friendly Version

Interactive Discussion



**Tropical Pangaeon  
Precipitation**

N. G. Heavens et al.

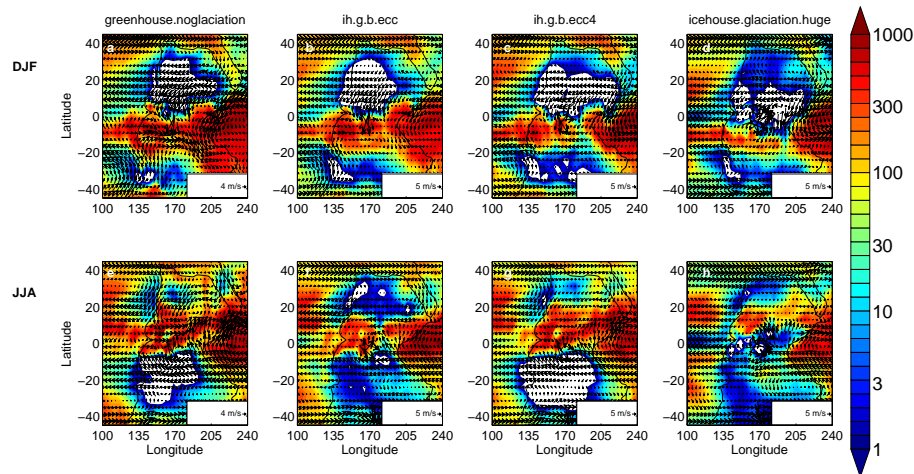


**Fig. 12.** Mean convective precipitation ( $\text{mm}$ ) and winds ( $\text{m s}^{-1}$ ), as labeled.

[Title Page](#)[Abstract](#)[Introduction](#)[Conclusions](#)[References](#)[Tables](#)[Figures](#)[◀](#)[▶](#)[◀](#)[▶](#)[Back](#)[Close](#)[Full Screen / Esc](#)[Printer-friendly Version](#)[Interactive Discussion](#)

Tropical Pangaeon  
Precipitation

N. G. Heavens et al.

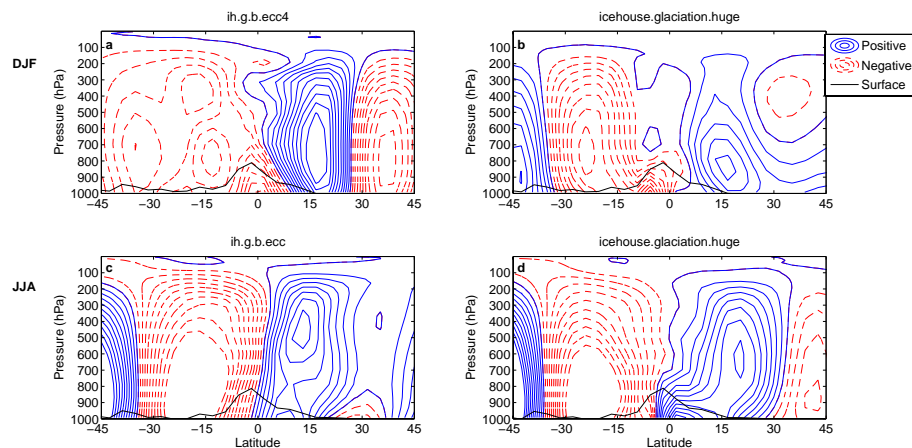


**Fig. 13.** Seasonal mean zonal average meridional streamfunction in the Pangaeon sector ( $146.25^{\circ}$ – $191.25^{\circ}$  longitude), as labeled. Plotting conventions are identical to those of Fig. 10.

Title Page

Abstract

Introduction

Conclusions

References

Tables

Figures

◀

▶

◀

▶

Back

Close

Full Screen / Esc

Printer-friendly Version

Interactive Discussion



**Tropical Pangaeon  
Precipitation**

N. G. Heavens et al.

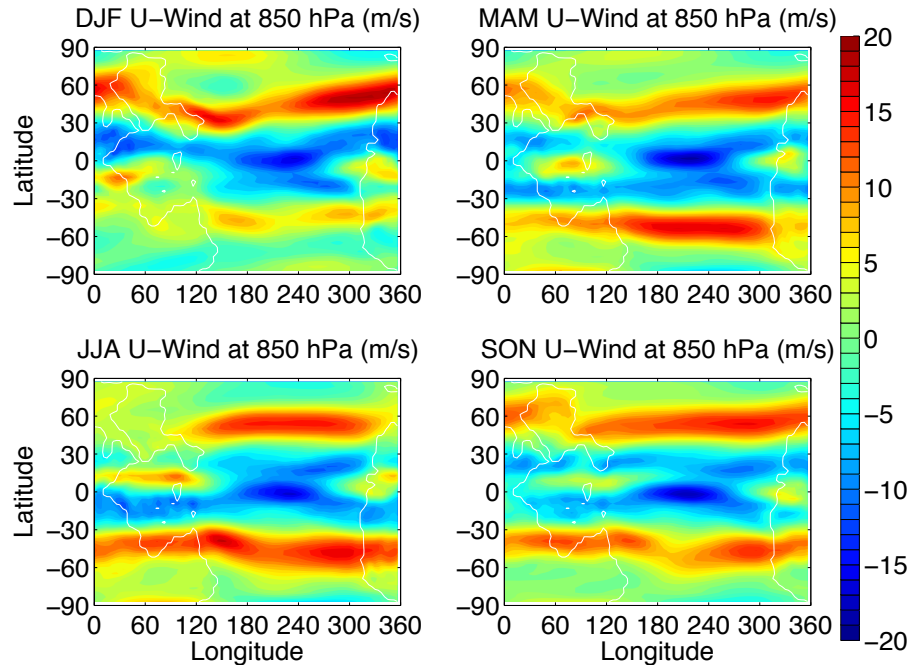


**Fig. 14.** Seasonal variability in mean zonal winds at 850 hPa ( $\text{m s}^{-1}$ ) in the Latest Permian Simulation of Kiehl and Shields (2005). Note that Paleo-Tethys is on the left side of each panel.

Title Page

Abstract

Introduction

Conclusions

References

Tables

Figures

◀

▶

◀

▶

Back

Close

Full Screen / Esc

Printer-friendly Version

Interactive Discussion



## Tropical Pangaeian Precipitation

N. G. Heavens et al.

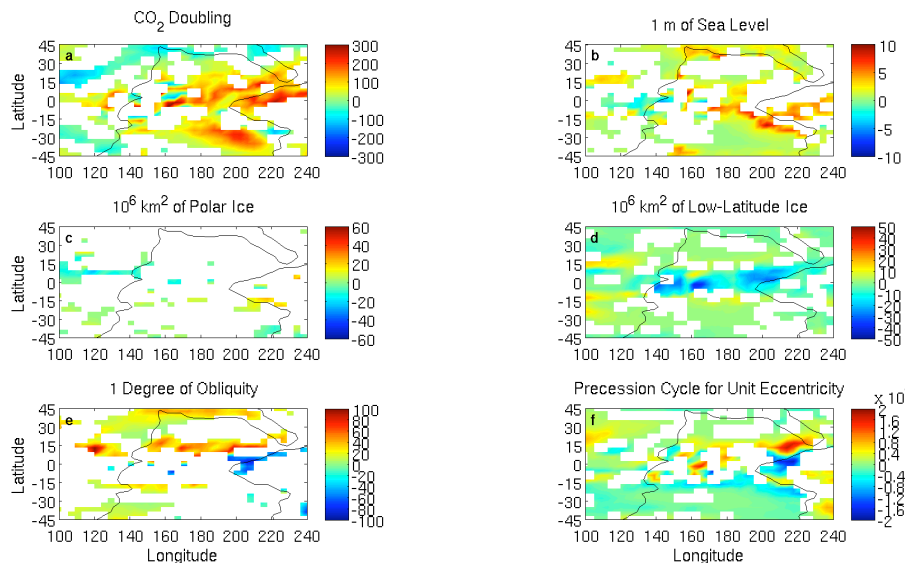


**Fig. 15.** Sensitivities of the simulation ensemble over tropical Pangaea, as described in the text and as labeled. Only sensitivities with amplitudes greater than twice the standard uncertainty estimated from inter-annual variability are plotted.

Title Page

Abstract

Introduction

Conclusions

References

Tables

Figures

◀

▶

◀

▶

Back

Close

Full Screen / Esc

Printer-friendly Version

Interactive Discussion



## Tropical Pangaeian Precipitation

N. G. Heavens et al.

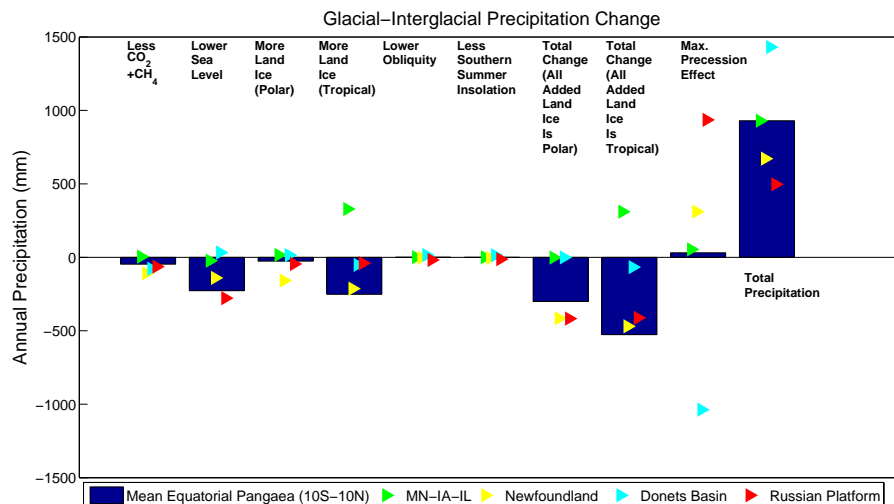


**Fig. 16.** Estimated change in precipitation in equatorial Pangaea and individual Pangaeian locations for a glacial phase relative to an interglacial phase. Precipitation sensitivity is estimated from Eqs. (1)–(5), while changes in greenhouse gas levels, sea level, land ice extent, and orbital parameters are estimated changes between the Last Glacial Maximum and the present day (Petit et al., 1999; Fairbanks, 1989; Peltier, 2004; Laskar et al., 2004). Individual locations plotted are named according to their approximate present-day locations: Illinois-Iowa-Minnesota ( $5.6^\circ$ ,  $161.25^\circ$ ); Newfoundland ( $1.9^\circ$ ,  $180^\circ$ ); Donets Basin ( $1.9^\circ$ ,  $217.5^\circ$ ); and the Russian Platform ( $16.7^\circ$ ,  $217.5^\circ$ ).

Title Page

Abstract

Introduction

Conclusions

References

Tables

Figures

◀

▶

◀

▶

Back

Close

Full Screen / Esc

Printer-friendly Version

Interactive Discussion



## Tropical Pangaeon Precipitation

N. G. Heavens et al.

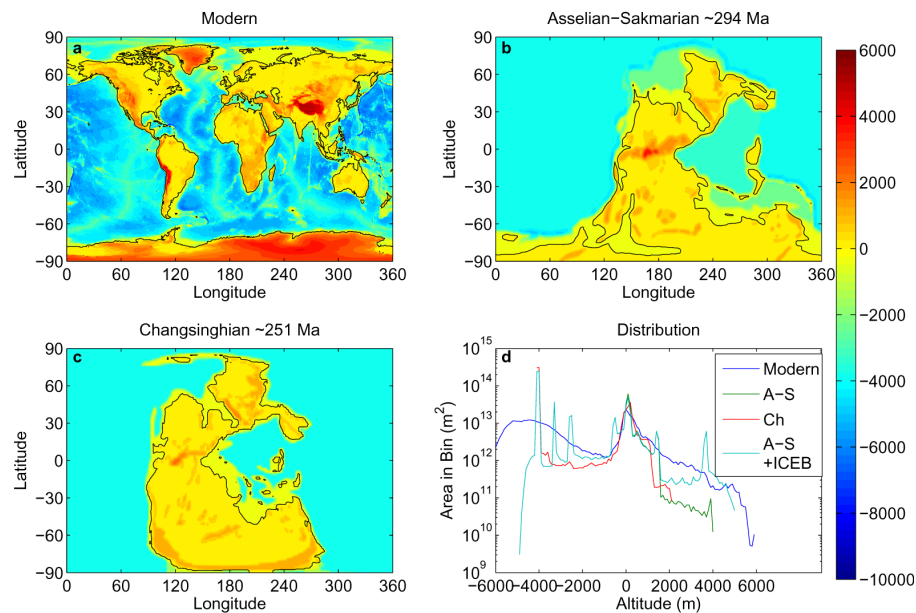


**Fig. A1.** (a–c) Digital elevation (m) models for the Earth for the present day (0 Ma) (NOAA NGDC, 2006); the Asselian-Sakmarian (299–284 Ma) (this study); and the Changhsingian (251 Ma) (Kiehl and Shields, 2005); (d) distribution of topography with altitude for the digital elevation models in (a–c) and the Asselian-Sakmarian map with the big polar glacial configuration (ICEB).

Title Page

Abstract

Introduction

Conclusions

References

Tables

Figures

◀

▶

◀

▶

Back

Close

Full Screen / Esc

Printer-friendly Version

Interactive Discussion

